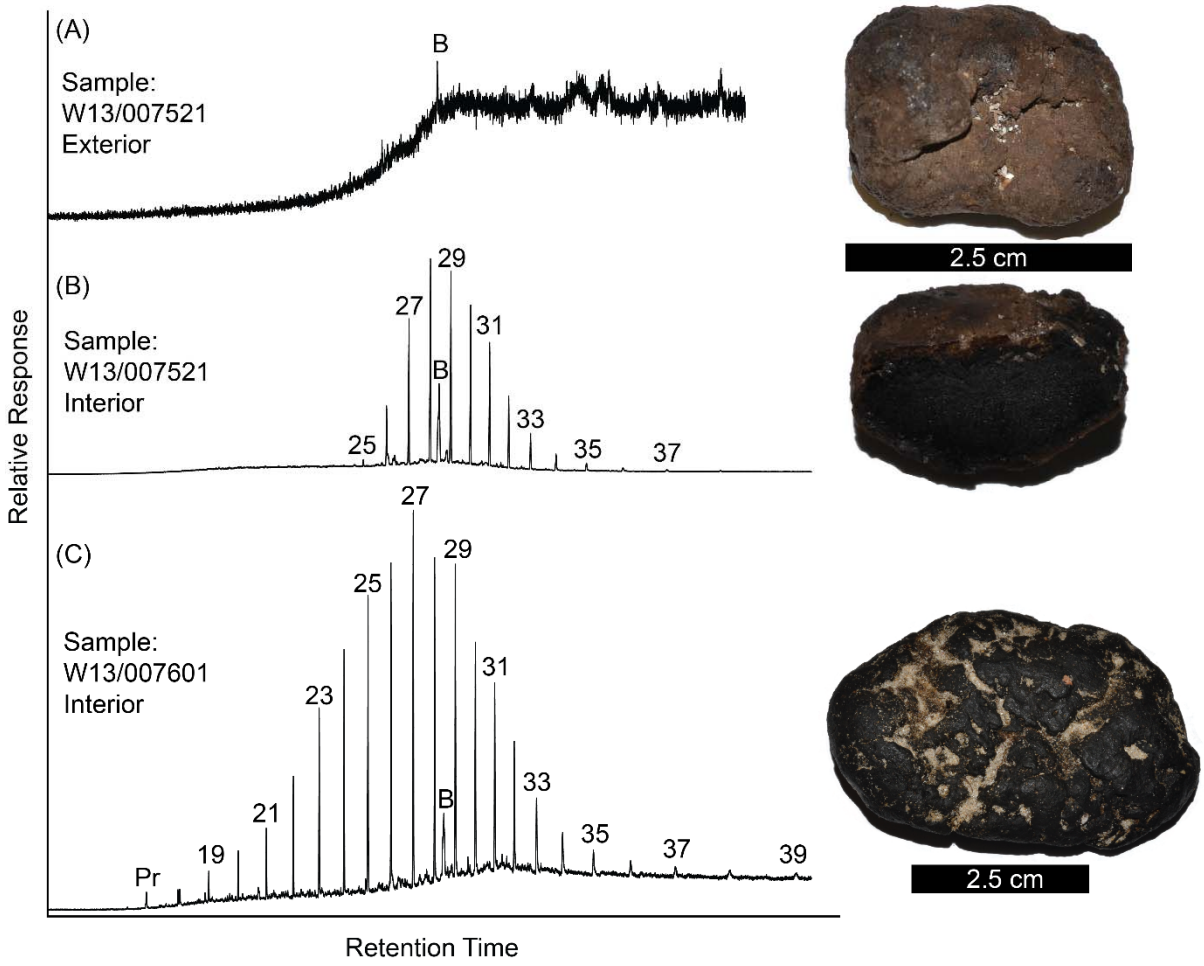

Figure 143: Example of GC-MS whole-oil degradation assessment using exterior vs. interior analysis. (A) Whole-oil GC-MS chromatogram of the exterior of extremely degraded Type I waxy bitumen W13/007521. (B) Whole-oil GC-MS chromatogram of the interior of sample W13/007521. (C) Whole-oil GC-MS chromatogram of the freshest example of the Type I waxy bitumen (W13/007601).

Degradation assessment based on lightest remaining n-alkane

All waxy bitumen specimens collected show some degree of *n*-alkane alteration. In highly degraded samples, all *n*-alkanes within the range of C_{10}-C_{39} have been completely removed. This allows a relative scale to be defined whereby samples in a given oil family may be ranked in order of alteration based on their lightest remaining *n*-alkane. This approach may be achieved employing the same whole-oil GC-MS geochemical screening data used to assign a specimen to a preliminary oil family, allowing for a rapid specimen classification and weathering assessment.

As the sequential loss of C_{12+} *n*-alkanes is largely attributed due to catabolism at differing rates by microbes, this scheme provides a useful preliminary assessment of biodegradation.

Degradation of Type I waxy bitumen (high botryococcane)

Type I waxy bitumen comprises the majority of the tarballs collected during the beach surveys and exhibit a wide range of degradation states, as summarized in Figure 144**.** This degradation range highlights the previously undocumented recalcitrance of the freshwater biomarker botryococcane (an acyclic C_{34} irregular isoprenoid alkane) to water washing and biodegradation. Its presence allows for identification of the Type I waxy bitumen, even after extensive degradation. Additionally, the ratio of botryococcane to the adjacent C_{29} *n*-alkane shows potential as a straightforward measure of biodegradation. However, this ratio is vulnerable to error in samples with a higher proportion of water washing (*n*-alkane drawdown) compared to biodegradation (sequential removal of *n*-alkanes). As a result, the preferred weathering assessment for the Type I waxy bitumen is the lightest preserved *n*-alkane.

The distribution of degradation states illustrated in Figure 144 (B) reveals approximately Gaussian (normal) distributions for samples collected each year, with a mean at n-C_{24} for samples collected in 2014/2016 and n-C_{25} in 2015. This indicates that on the defined relative degradation scale (i.e. freshest to most degraded), most of the collected samples may be considered moderately degraded.

Historical continuity

The high abundance of botryococcane makes this unique family of waxy bitumen clearly identifiable with that reported in previous studies (Padley, 1995; Edwards et al., 2016, 2017). The similarity of such waxy bitumen collected in 1960 with equivalent samples collected in 1990 demonstrated the strong continuity of such strandings. While these previously collected tarballs contain *n*-alkanes as light as C_{11} or C_{12} and the intact source-specific isoprenoid biomarkers pristane (Pr) and phytane (Ph), samples collected during the GABRP are significantly more degraded than their historical equivalents (Figure 145). Thus the freshest example of a high-botryococcane waxy bitumen (W13/007601) lacks *n*-alkanes $<C_{17}$ and Pr and Ph are highly depleted.

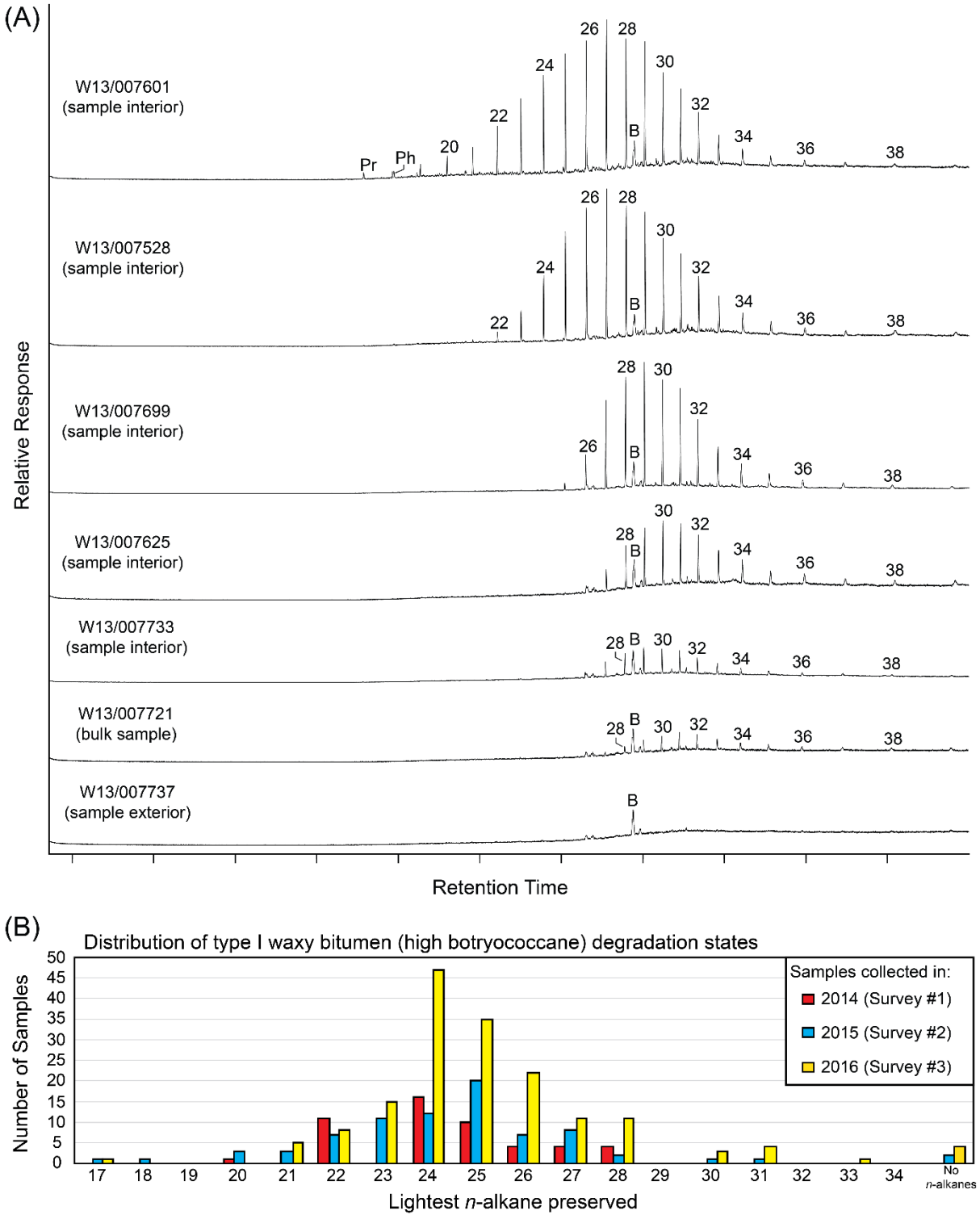

Figure 144: Degradation overview for Type I waxy bitumen (high botryococcane). Each chromatogram is scaled such that no compound which is not a product of biodegradation may have a higher response than the freshest sample. (A) Representative examples of degradation states revealed by whole-oil GC-MS analysis. (B) Histogram plot of the lightest preserved *n*-alkane from each beach survey.

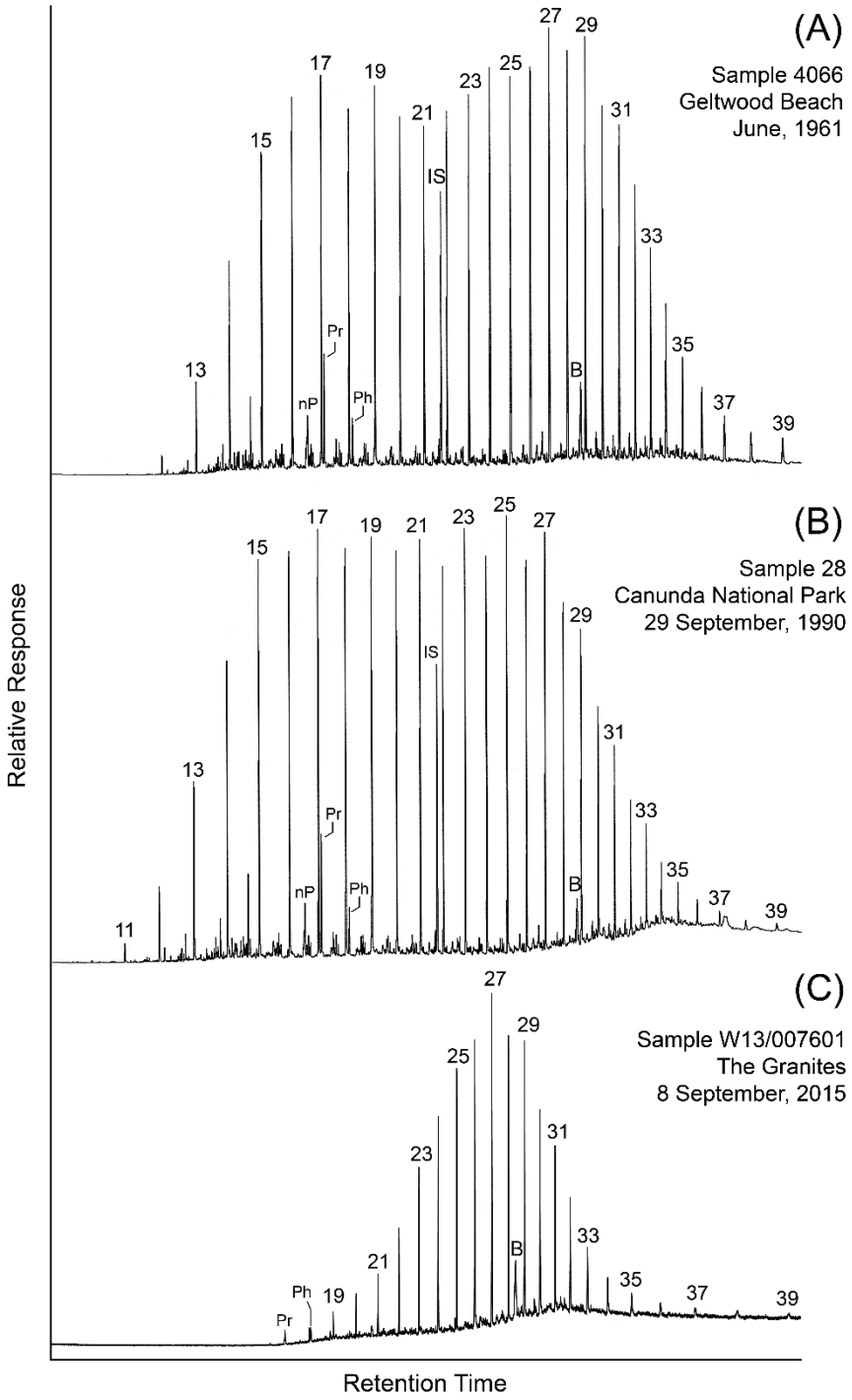

Figure 145: Historical continuity of Type I waxy bitumen stranding: (A) Sample 4066 collected in 1961 and analysed by Padley (1995). (B) Sample 28 collected in 1990 and analysed by Padley (1995). (C) Sample W13/007601 collected in 2015 during the second coastal survey of the GABRP. This specimen is the freshest example of Type I waxy bitumen collected between 2014 and 2016. Abbreviations: Np = norpristane, Pr = pristane, Ph = phytane, B = botryococcane, IS = internal standard of 3-methylheneicosane used by Padley (1995), numbers = *n*-alkane chain lengths.

Degradation of Type II waxy bitumen (low botryococcane)

Type II waxy bitumen is the least abundant variety of tarball. Even so, significant variation in the extent of *n*-alkane degradation was observed in the collected specimens (Figure 146A). Whereas the freshest example (sample W13/007615) contains remnant pristane and phytane, in the majority of samples these components are completely lost. Due to the small number of samples collected, a confident assessment of the distribution of degradation states in this family (Figure 146B) is not possible.

Historical continuity

As for Type I waxy bitumen, the prescence of botryococcane makes this family easily recognizable as one of those described by Padley (1995) and Edwards et al., (2016, 2017). Comparison of the freshest sample found during the 2014-2016 GABRP with those collected in 1983 and 1990 shows that the recently stranded Type II waxy bitumens are more degraded than their historical counterparts (Figure 147).

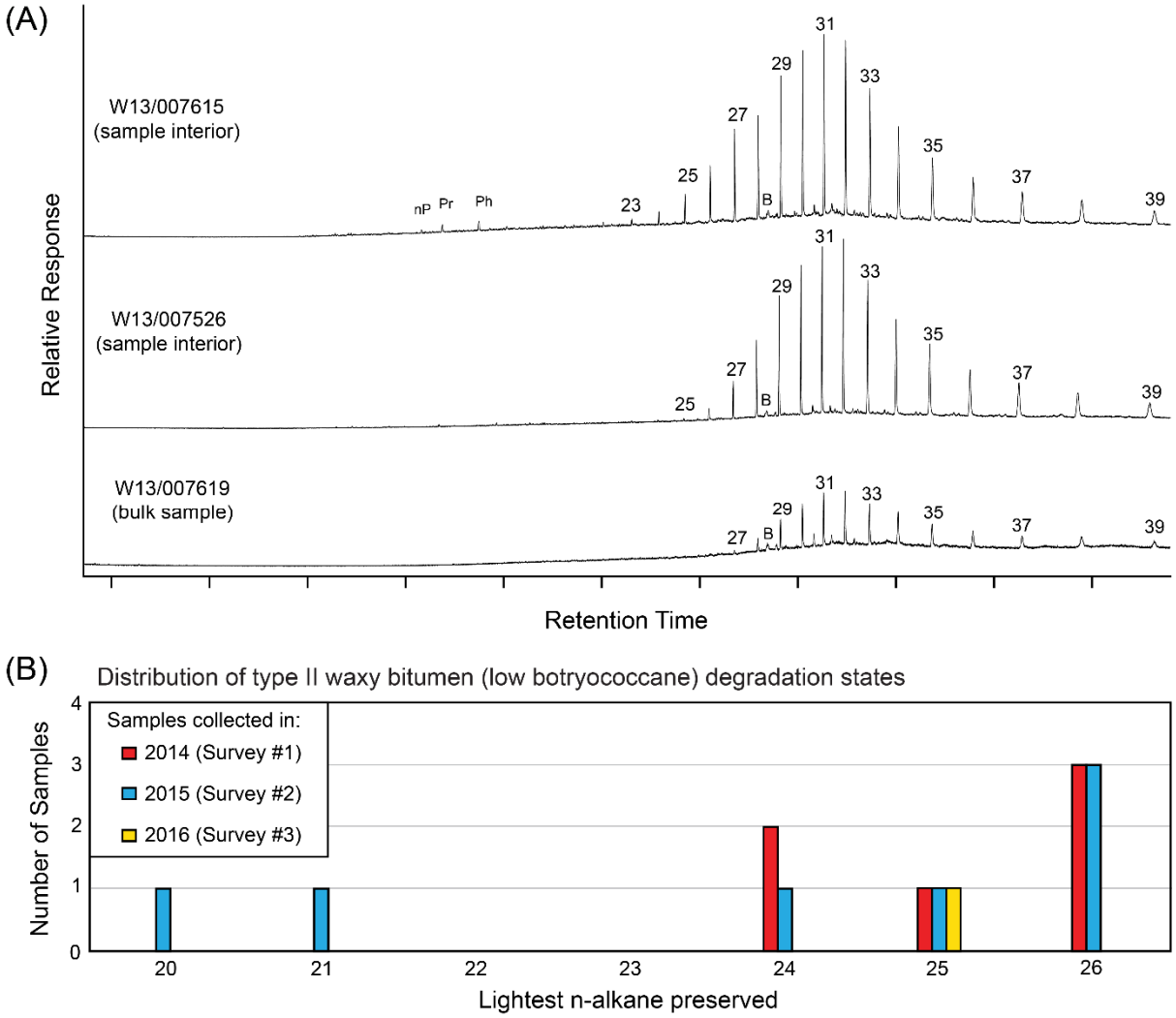

Figure 146: Degradation overview for Type II waxy bitumen (low botryococcane). Each chromatogram is scaled such that no compound which is not a product of biodegradation may have a higher response than the freshest sample. (A) Representative examples of degradation states revealed by whole-oil GC-MS analysis. (B) Histogram plots of the lightest preserved n-alkane from each beach survey.

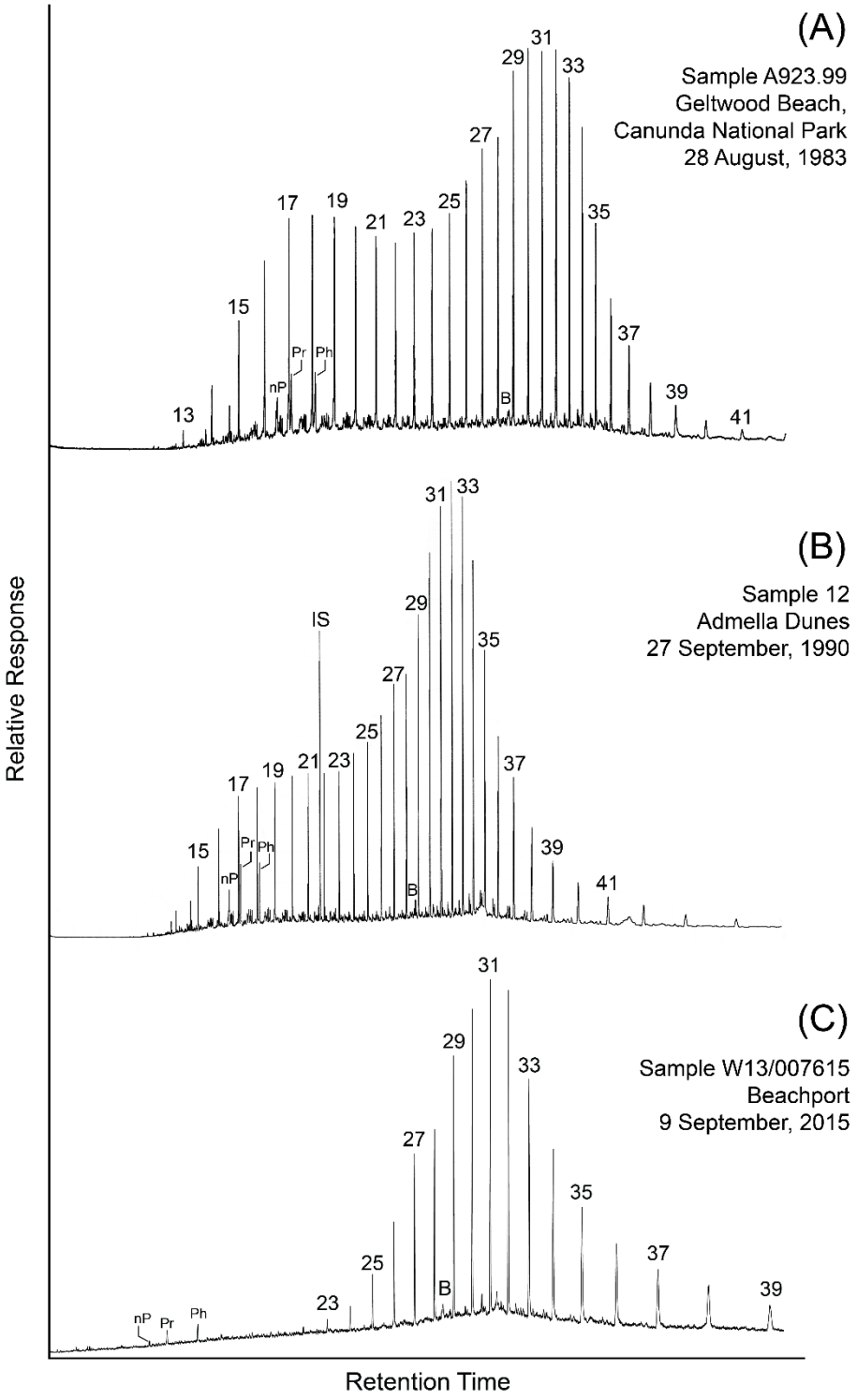

Figure 147: Historical continuity of Type II waxy bitumen stranding. Each chromatogram is scaled such that no compound which is not a product of biodegradation may have a higher response than the freshest sample. (A) Sample A923.99 collected in 1983 and subsequently analysed by Padley (1995). (B) Sample 12 collected in 1990 and analysed by Padley (1995). (C) Sample W13/007615 collected in 2015 during the second survey of the GABRP. This specimen is the freshest example of type II waxy bitumen collected

between 2014 and 2016. Abbreviations: Np = norpristane, Pr = pristane, Ph = phytane, B = botryococcane, IS = internal standard of 3-methylheneicosane used by Padley (1995), numbers = *n*-alkane chain lengths.

Degradation of Type III waxy bitumen (no botryococcane, low wax)

Type III waxy bitumen is the second most abundant variety of tarballs and it includes the best-preserved samples. The representative range of degradation states for the Type III waxy bitumen is shown in Figure 148A. Fresh specimens contain *n*-alkanes as light as C_{12} and intact pristane and phytane. As the extent of degradation increases the latter two components are shown to progressively diminish before near-complete loss occurs.

The distribution of degradation states is shown in Figure 148B. Overall each year's sample population shows a bimodal distribution of degradation states, with samples collected in November 2014 notably more degraded than their counterparts collected in September 2015 and Ocytober 2016. The increased degradation may be the result of the bitumen strandings shaving spent longer on the beach than did those collected in later surveys. However, it should also be noted that if seasonality were the predominant driver of this difference, then other waxy bitumen families would likewise be expected to show a similar systematic increase in alteration in the 2014 collection. This is not observed.

Furthermore, the presence of multiple oil families on the basis of source-specific biomarkers (Types IIIA – E) makes an accurate assessment of the range of degradation for each family impossible without identifying the oil family of every specimen on the basis of their biomarker geochemistry.

Historical continuity

Waxy bitumen lacking the biomarker botryococcane have previously been considered a single oil family. However, analysis of waxy bitumens lacking botryococcane in this study have revealed a wide range of different oil families. As a result, it is not possible to directly compare the degradation state of these waxy bitumens without reassessing a large number of historical samples.

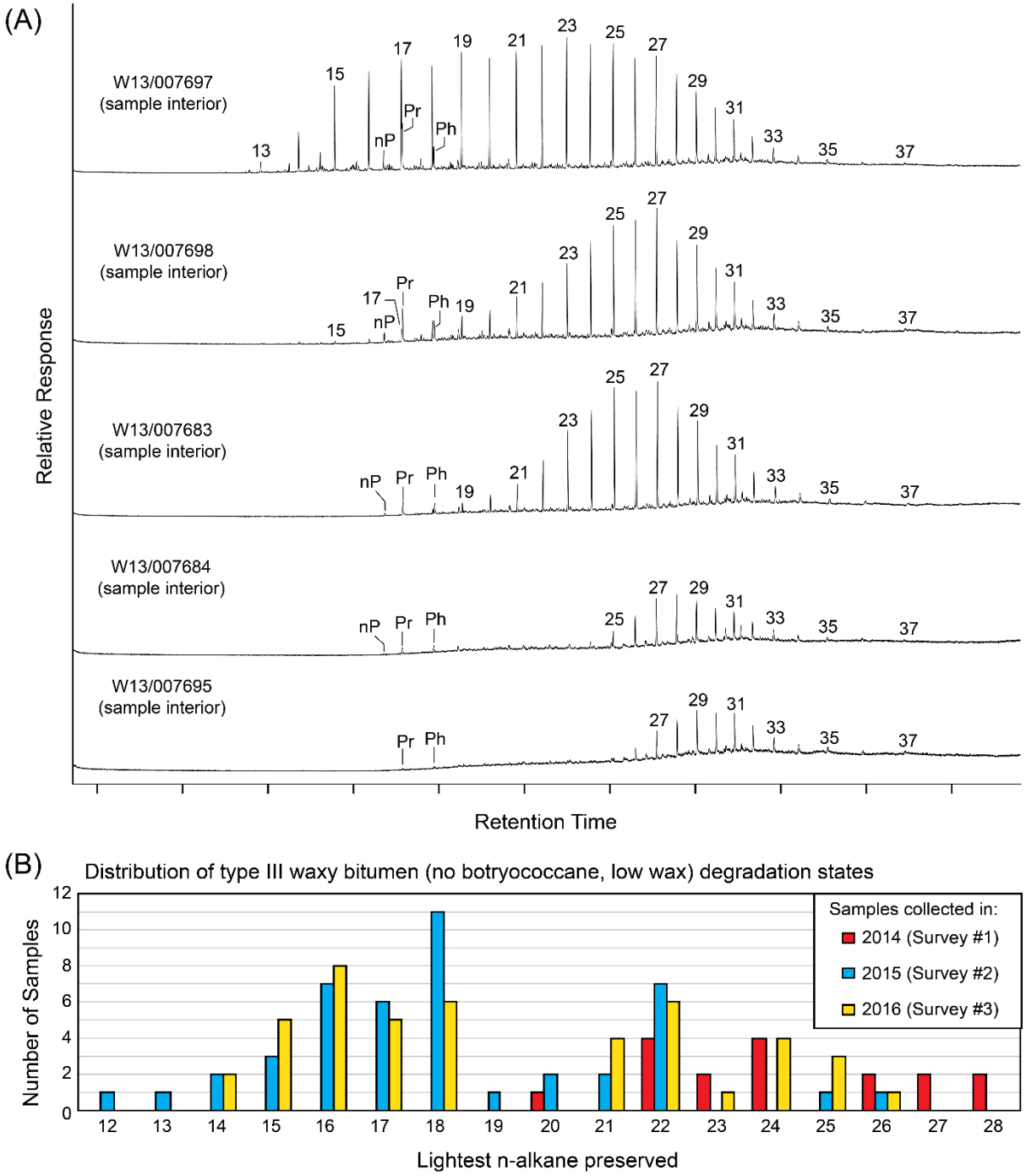

Figure 148: Degradation overview for Type III waxy bitumen (no botryococcane, low wax). Each chromatogram is scaled such that no compound which is not a product of biodegradation may have a higher response than the freshest sample. (A) Representative examples of degradation states revealed by whole-oil GC-MS analysis. (B) Histogram plots of lightest preserved *n*-alkane from each annual survey.

Degradation of Type IV waxy bitumen (no botryococcane, high wax)

Type IV waxy bitumen is the less common variety of waxy bitumen lacking the freshwater biomarker botryococcane. Its range of degradation states is shown in Figure 149A. The freshest examples contain *n*-alkanes as light as C_{15} with intact or minimally depleted pristane and phytane. However, in most specimens these latter components are highly altered or completely removed.

The distribution of these degradation states is shown in Figure 149B. The low number of samples recovered from this oil family results in an inconsistent distribution pattern. Additionally, the identification of multiple oil families on the basis of source-specific biomarkers (Types IVA-E) makes an accurate assessment of the range of degradation for each family impossible without identifying the oil family of every specimen on the basis of their biomarker geochemistry

Historical continuity

In the same manner as the Type III waxy bitumens, the discovery of multiple oil families lacking the biomarker botryococcane which have not been identified in previous surveys prevents a practical assessment of the historical continuity of weathering extent. In order to establish this continuity, all waxy bitumens which lack botryococcane would need to be sorted into the biomarker-defined oil families prior to establishing a full range of degradation states. This is not practical given the high number of coastal bitumens classified as either Type III or Type IV.

Miscellaneous types of coastal bitumen (unknowns, unclassified high wax bitumen)

Analysis of source-specific biomarkers of several unclassified high-wax bitumens revealed that many examples are highly degraded Type IVA waxy bitumen. Further assessment of these bitumens and many of the highly degraded bitumens classified as 'Unknown', is required to ascertain if any of the remaining samples represent oil families unidentified in the current dataset. However, due to the extent of biodegradation affecting source-specific biomarkers in these samples, an accurate assessment and identification may not be possible in all cases.

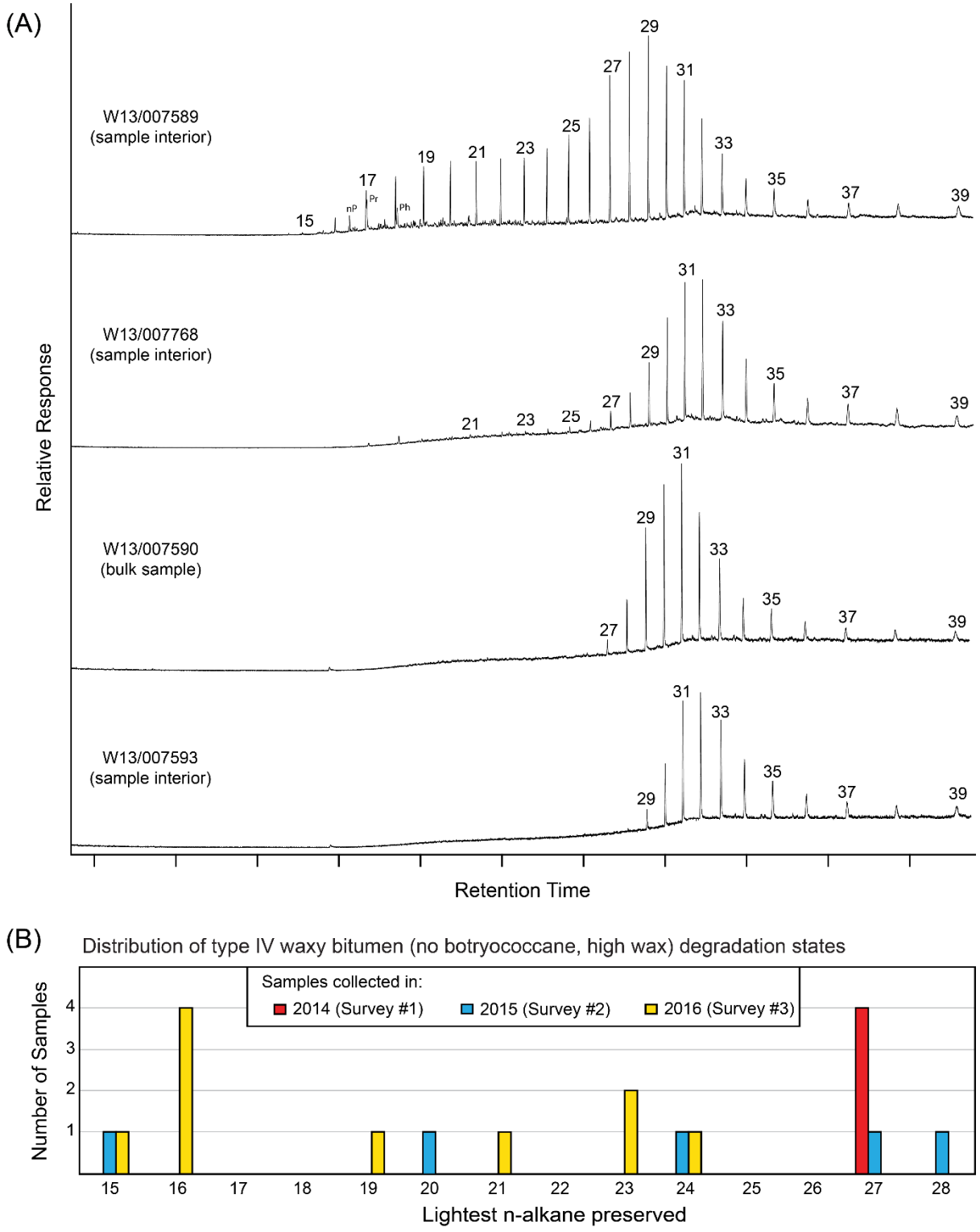

Figure 149: Degradation overview for Type IV waxy bitumen (no botryococcane, high wax). Each chromatogram is scaled such that no compound which is not a product of biodegradation may have a higher response than the freshest sample. (A) Range of degradation states revealed by whole-oil GC-MS analysis. (B) Histogram plots of their lightest preserved *n*-alkane from each annual survey.

Waxy bitumen biomarker degradation

The waxy bitumen families exhibit a wide range of degradation states. The progressive degradation of steranes/diasteranes and terpanes are shown in Figure 150 and Figure 151, respectively. Similar to the non-traditional sequence of biodegradation identified in the asphaltites, the waxy bitumen similarly show diasterane alteration and removal prior to the complete removal of the C_{27}-C_{30} ααα 20 R steranes (Figure 150). Although the comparison using Type I waxy bitumen contains relatively low response for diasteranes, the C_{27} βα diasteranes show significant alteration in comparison to the high response of the recalcitrant tetracyclic polyprenoid doublet peak (TPP).

The *m/z* 191 chromatograms shown in Figure 151 illustrate the prominent alteration/drawdown of the maturity-dependent C_{27} triterpane, Tm, the C_{29} αβ hopane (becoming < C_{27}Ts) and the C_{30} αβ hopane. Minor alteration and drawdown also affects the C_{19}-C_{23} tricyclic terpanes (19/3 to 29/3) and the C_{24} tetracyclic terpane (24/4). However, the highly degraded waxy bitumen exhibits less degradation than that observed in the highly degraded asphaltites where these compounds have been removed entirely.

This similar pattern of alteration, progressively removing compounds on the basis of carbon number, is also observed in other families of waxy bitumen. The recognition of these degradation sequences may permit identification of extremely degraded samples. However, compound ratios from samples which display prominent alteration of to their biomarker composition should not be considered representative of the parent source rock and hence should not be used for correlation purposes. Furthermore, given that fresher examples of these bitumens are recognised, this alteration can be assigned to degradation processes in the marine environment, rather than to biodegradation in the reservoir or during migration to the seafloor.

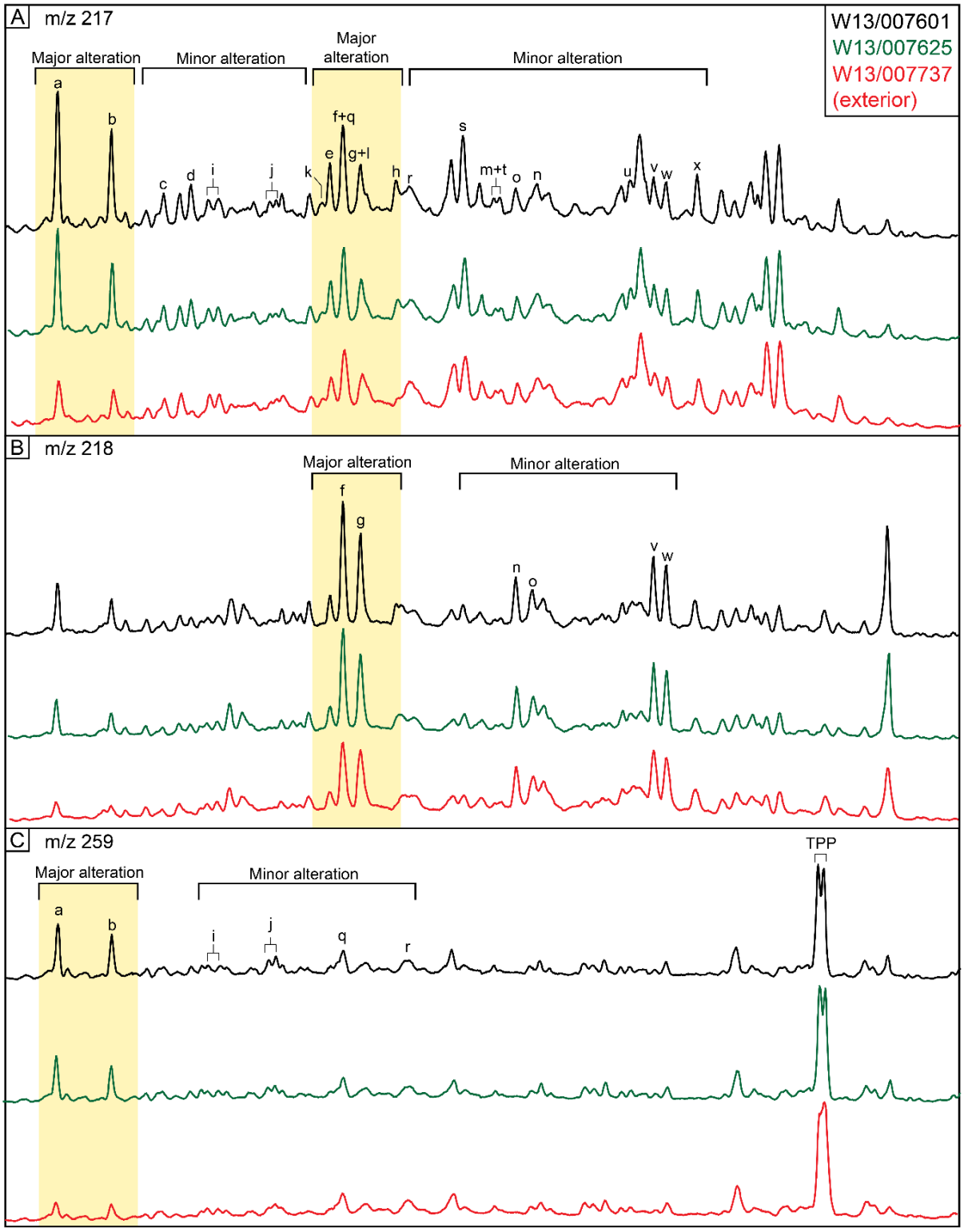

Figure 150: Summary of sterane and diasterane degradation in Type I waxy bitumen from the freshest identified sample (W13/007601) to a highly degraded sample (W13/007737). Each chromatogram is scaled such that no compound which is not a product of biodegradation may have a higher response than the freshest sample. (A) Sterane and diasteranes degradation observed in *m/z* 217 chromatogram. (B) Degradation of C_{27}-C_{29} αββ steranes observed in the *m/z* 218 chromatogram. (C) Degradation of C_{27}-C_{29} βα diasteranes observed in the *m/z* 259 chromatogram. For peak identifications refer to table 19.

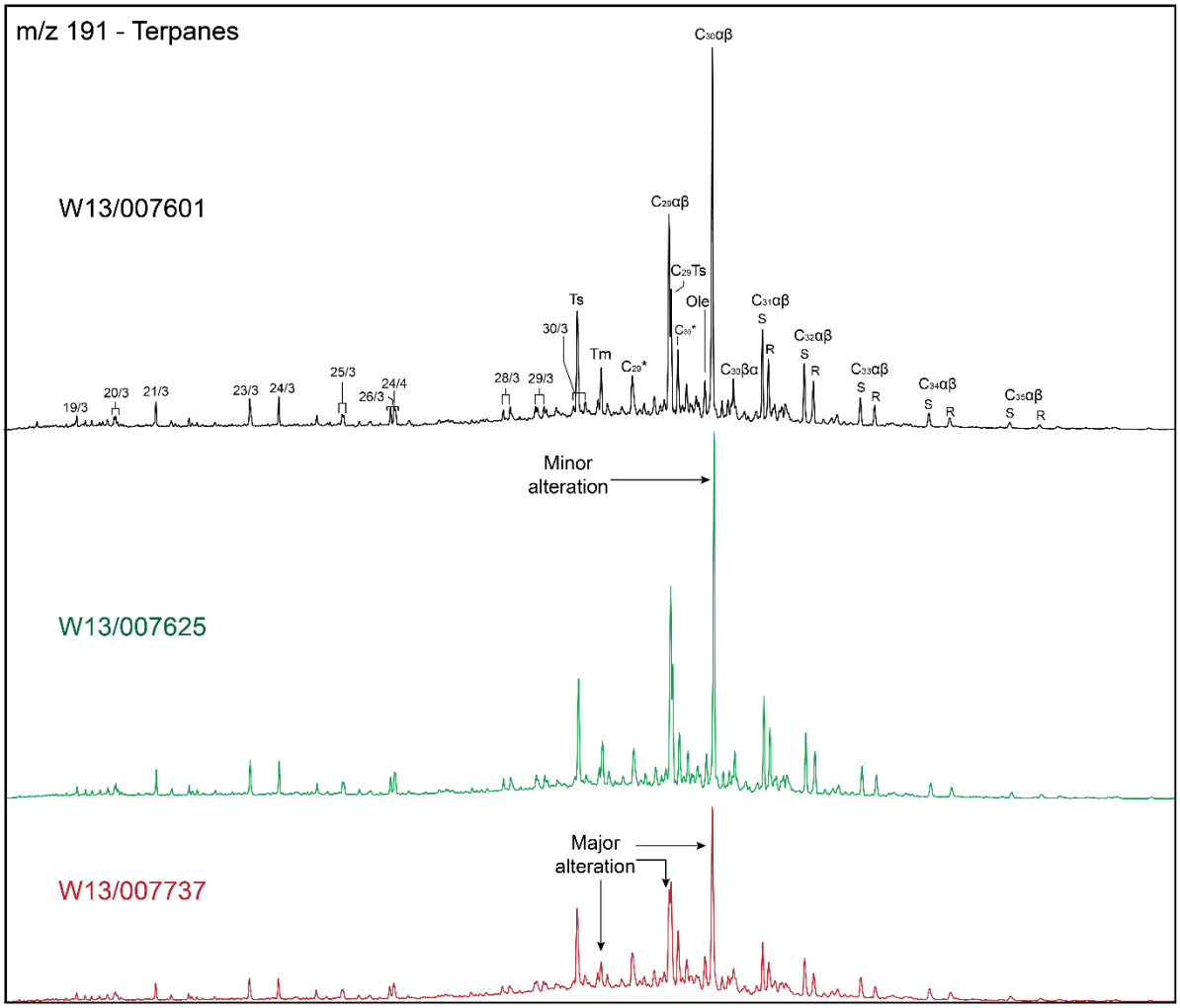

Figure 151: Summary of terpane degradation in Type I waxy bitumen from the freshest identified sample (W13/007601) to a highly degraded sample (W13/007737) using the *m/z* 191 chromatogram. Each chromatogram is scaled such that no compound which is not a product of biodegradation may have a higher response than the freshest sample. For peak identifications refer to table 19.

Summary and conclusions

An assessment of the level of degradation of coastal bitumen is necessary to understand 1) how to identify each oil family despite varying degrees of weathering, and 2) the historical evolution of each family with a view to assessing its environmental impact. It is preferable to use the stranding locations of only the fresh specimens for oceanographic provenance modelling.

The best approach to the assessment of degradation in coastal bitumen is to identify those samples in each oil family that still contain low-molecular-weight compounds susceptible to alteration and/or removal. This can be achieved using whole-oil GC-MS. However, it does require the analysis of all collected samples in order to identify the full range of degradation states. In examples where the oil family is clearly identified from whole-oil GC-MS screening (e.g. Type I and II bitumens), this is straightforward. In samples which require a complete biomarker assessment to determine their oil family (e.g. Type IIIA-E and Type IVA-E families), establishing a complete range of degradation states is not possible without analysing the biomarker geochemistry of all collected specimens, which is not

practical given the high number of samples collected. The ranges of degradation defined here for the asphaltites and Type I/II waxy bitumens will likely be of use to characterise the extent of degradation in any bitumen samples collected in future surveys.

The continued stranding of soft, fresh asphaltite specimens supports the notion of an active and local seep in the GAB. Additionally, the majority of asphaltites show minimal degradation of the steranes and terpanes used for oil-oil and oil-source correlation. Alteration is only observed in the extremely degraded asphaltite samples collected from Tractor Beach.

Comparison of samples collected in 2014–2016 with archival specimens reveals that the Type I and II waxy bitumens transported from Indonesia are far more degraded than their predecessors from the 1990s and prior. This increased degradation, in combination with far lower levels of modern hydrocarbon loading (discussed in BEACH SURVEY DATA), suggests that the input of Southeast Asian crude oil to the GAB region via the Leeuwin Current has significantly declined. We interpret this to signify either a diminution in Indonesian seep activity or improved maritime practices in the transportation of crude oil.

The increased degradation of Indonesian-derived waxy bitumen also questions the viability of using modern stranding locations for oceanographic provenance modelling. The waxy bitumen collected between November 2014 and October 2016 has likely been migrating throughout the GAB for too long to accurately model. However, the continued stranding of soft, fresh asphaltite specimens supports the notion of a local source, most likely a local seep in the Bight Basin. Given the number of fresh asphaltite strandings, oceanographic modelling of the asphaltites may still provide useful information.

Finally, comparison of the range of degraded coastal bitumens has revealed highly non-traditional biodegradation pathways for crude oil in the ocean. Specifically, this is shown in the degradation of diasteranes, typically thought to degrade only after complete removal of the C_{27}-C_{29} steranes.

GEOCHEMISTRY SUMMARY AND CONCLUSIONS

Characterisation of the large suite of coastal bitumens (n = 631) collected during the GAB Research Program Project 5.2 involved their physical documentation (photography, measurement and weighing) followed by initial geochemical screening employing bulk elemental (C, H, N, S) and whole-oil GC-MS analyses. This enabled the recognition of different oil families, representative examples of which then underwent detailed analysis by bulk IRMS ($\delta^{13}C$, $\delta^{34}S$), SIM GC-MS, GC-MS-MS, HT-GC-MS and CSIA to identify their source-specific isotopic and biomarker signatures. Finally, the acquired geochemical data were subjected to hierachical cluster analysis to assess the degree of difference between the oil families.

The principal findings of this phase of the project may be summarised as follows:

- Fifteen oil families and sub-families were distinguished on the basis of their physical properties and biomarker geochemistry, two asphaltic (one hard and one soft) and thirteen

varieties of waxy bitumen; significantly more than the six families of South Australian coastal bitumen known from previous studies.

- As a population of stranded oil residues, the waxy bitumens differ from those found along the same coastline between 1960 and 1995 in being much more weathered and biodegraded, consistent with both their smaller size and lesser numbers.
- The soft asphaltic bitumen recovered from Number 1 & 2 Rocks on the Limestone Coast is unique, and likely represents an early expulsion product from a Cretaceous marine source rock similar to that which gave rise to the asphaltites. Both may be evidence of a local active petroleum system in the Bight Basin.
- The vast majority (but not all) of the waxy bitumens (tarballs) have distinctive Cenozoic biomarker signatures that point to their origin from distant offshore oil seeps in the Indonesian Archipelago.
- The decline in abundance of stranded waxy bitumen over the past 20+ years attests to a diminution of seep activity and/or improved environmental practices related to tanker washing and oil spillage within Indonesian waters.
- At least two of the waxy bitumen sub-families that lack these Indonesian signatures (Type IV D & E) are of marine carbonate source affinity and could therefore originate from seeps in offshore basins along Australia's western and southern continental margin.
- The analysis of multiple, variously weathered samples from the same family of waxy bitumen has revealed unique, non-text book biodegradation pathways for crude oil in the ocean.
- This previously unrecognised complexity in the number of petroleum systems which impact the South Australian coastline has potentially important implications for the prospectivity of its offshore basins. Suggesting the presence of previously unrecognised active petroleum systems in the region.
- Further seep identification work is required to validate the proposed oil family classification.

Part 4 Oceanography

IMPLICATIONS OF METOCEAN CONDITIONS OF THE GAB ON ASPHALTITE AND TARBALL STRANDINGS

Introduction to metocoean conditions of the Great Australian Bight

The major metocean conditions in the Great Australian Bight (GAB) have been previously reviewed prior to this project by Rogers et al., (2013) and are summarised below to aid the understanding of the major processes affecting tarballs and asphaltites on their journey to their ultimate stranding locations.

Meteorological conditions of the Great Australian Bight

During summer, a large high-pressure system typically dominates the meteorology of the greater GAB as illustrated in Figure 152. The system in turn drives an anti-cyclonic wind stress field similar to the February averaged climatology shown in Figure 153 (Trenberth et al., 1989). The high pressure system and anti-cyclonic winds are punctuated by the occasional passage of cold fronts that lead to westerly winds and localised cooling. Wind variability is summarised by the standard deviation of the alongshore component of wind stress (0.1 Pa.), that is twice the mean (0.05 Pa, Table 40). The sea breeze can also reach 10 m/s at the Head of the Bight due to the strong differential in sea-surface and terrestrial temperatures. Observed conditions also show winds and a lack of variability in prevailing wind direction throughout the summer months of 2014 (Figure 154).

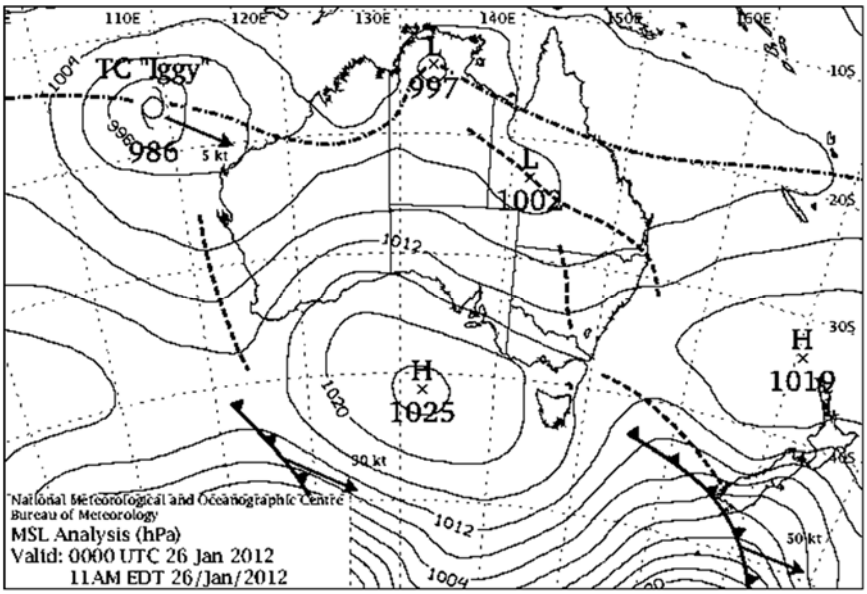

Figure 152: Mean sea level pressure (M.S.L.P units hPa) for Australia on 26th January 2012. Winds for the SA region are directed to the northwest.

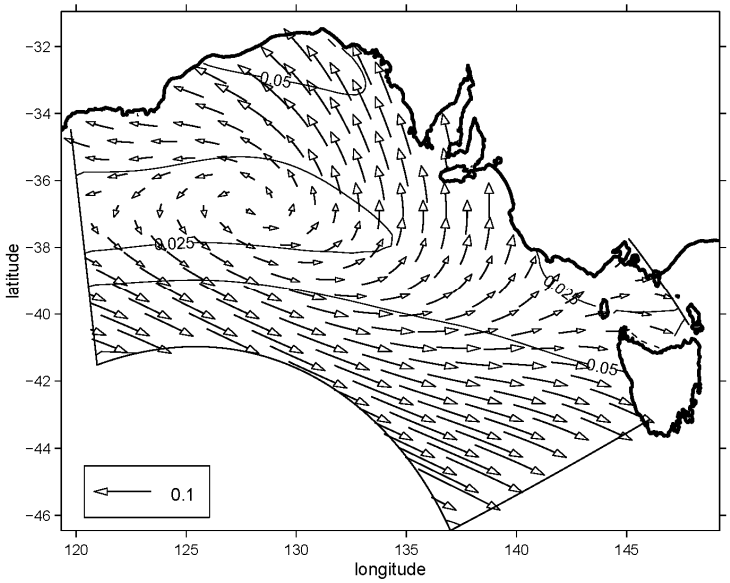

Figure 153: February average of wind stress obtained (after Trenberth et al., 1989). The vector indicated has a magnitude of 0.1 Pa and the contours of wind stress with magnitudes of 0.025 Pa and 0.05 Pa are indicated, (from Middleton & Platov, 2003).

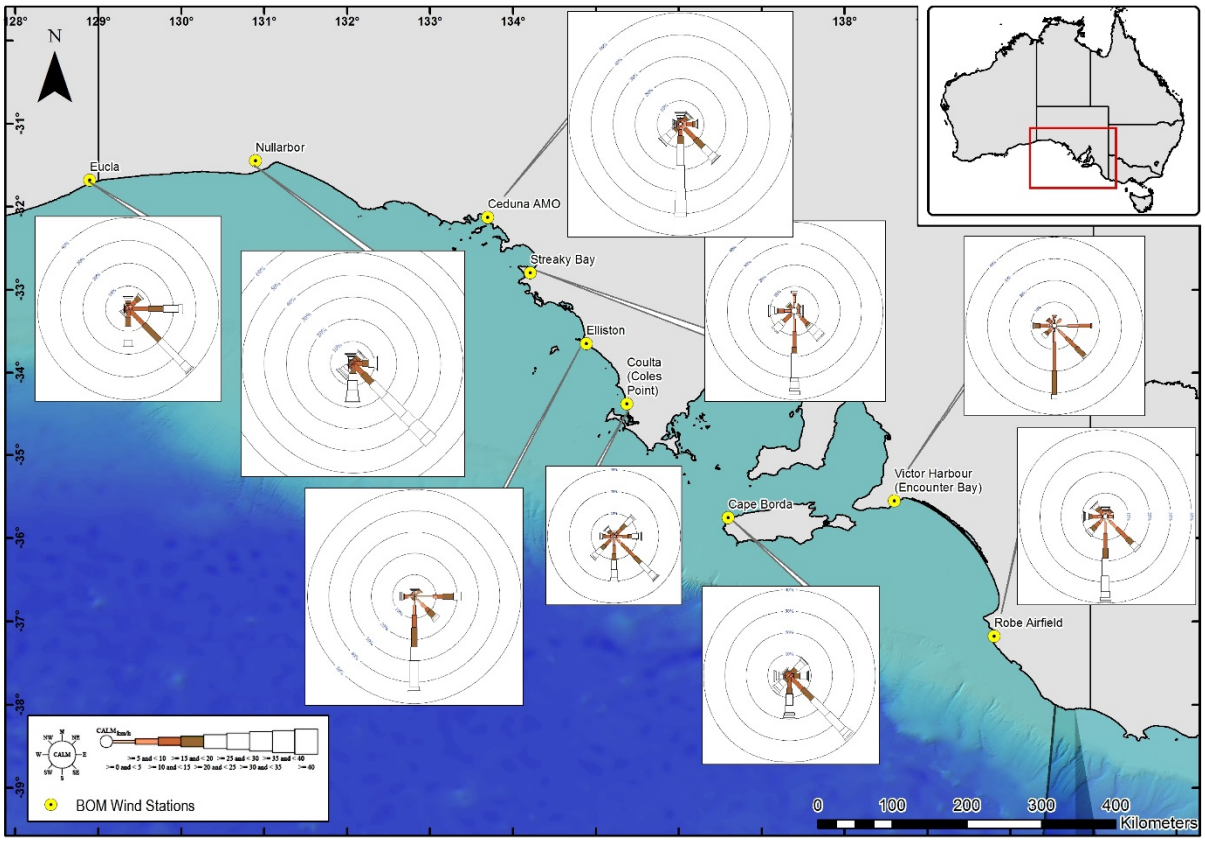

Figure 154: Average winds measured by coastal weather station for January-February-March 2014.

The high-pressure system is in part maintained by the sea-surface temperatures that are cooler than the southern Australian land mass to the north. The cooler sea-surface temperatures in turn cool the atmosphere, making it denser and reinforcing the high-pressure system itself. During winter the converse holds and the land-surface temperatures are cooler than the ocean. The high pressure migrates to the north allowing for greater passage of cold fronts near the coast (Figure 155) and the zonal eastward winds shown in Figure 155 and Figure 156. The winds increase in magnitude with latitude. The intense storms lead to greater variability with seasonal maxima in the wind stress (speed) of 1.1 Pa (23 m/s: Table 40). Localised observed conditions in 2014 also show a large variability in wind speed and direction when compared to the summer conditions (Figure 157).

Table 40: Typical values of the south-easterly components of the mean and standard deviation (S. Dev.) of the wind stress: units Pascals. The similar statistic is presented in brackets but for the corresponding wind speed in m/s: 10 m/s = 36 km/hr. A positive mean is directed to the south-east along the shelf. The maximum wind stress most likely to be experienced in any year is also given and was inferred from Trenberth et al., (1989). The heat fluxes are from the NCAR/NCEP (Kalnay et al., 1996) climatology for the GAB while those in brackets are for the Head of the Bight (Herzfeld, 1997).

QUANTITY	SUMMER: DEC. - FEB.	WINTER: JUNE – AUGUST
Mean Wind stress (wind)	-0.05 (7)	0.07 (8)
S. Dev. wind Stress (wind)	0.1 (9.3)	0.12 (10)
Season Maxima stress (wind)	0.2 (12)	1.1 (23)
Heat Flux (W m $^{-2}$)	50 (100)	-100 (-20)

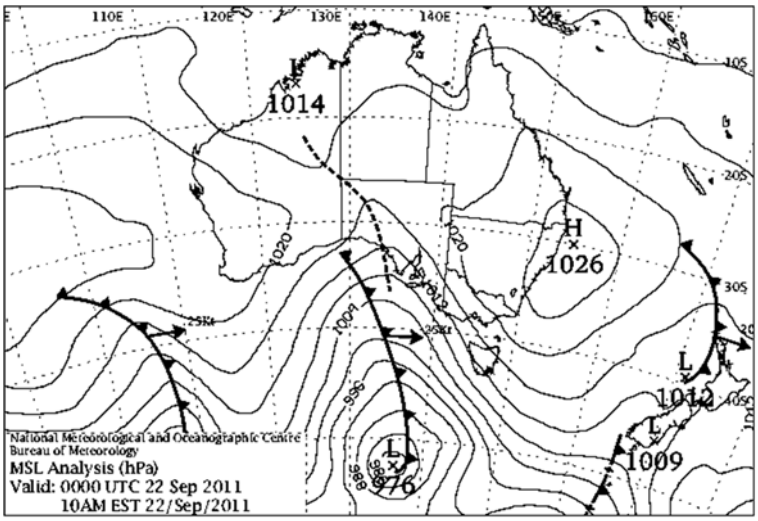

Figure 155: M.S.L.P. (units hPa) for Australia for the 22nd September 2011. Winds for the SA region are directed to the east.

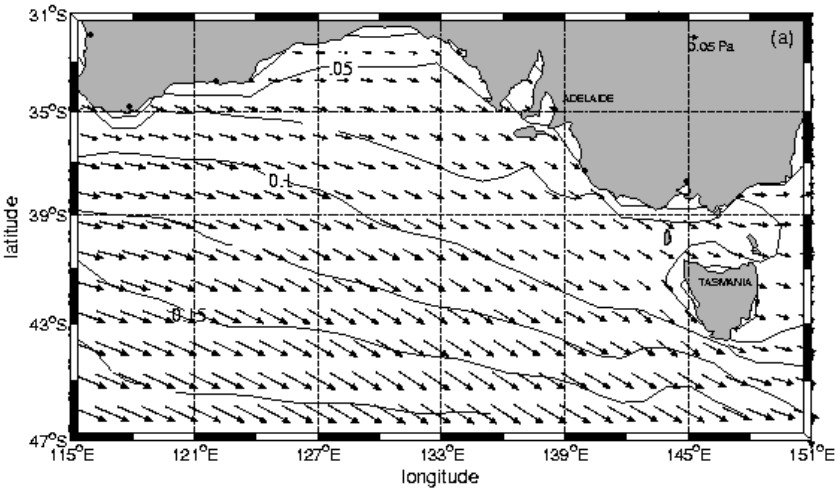

Figure 156: Wind mean wind stress field for winter. A legend vector of 0.05 Pa is indicated (Middleton and Cirano, 2002).

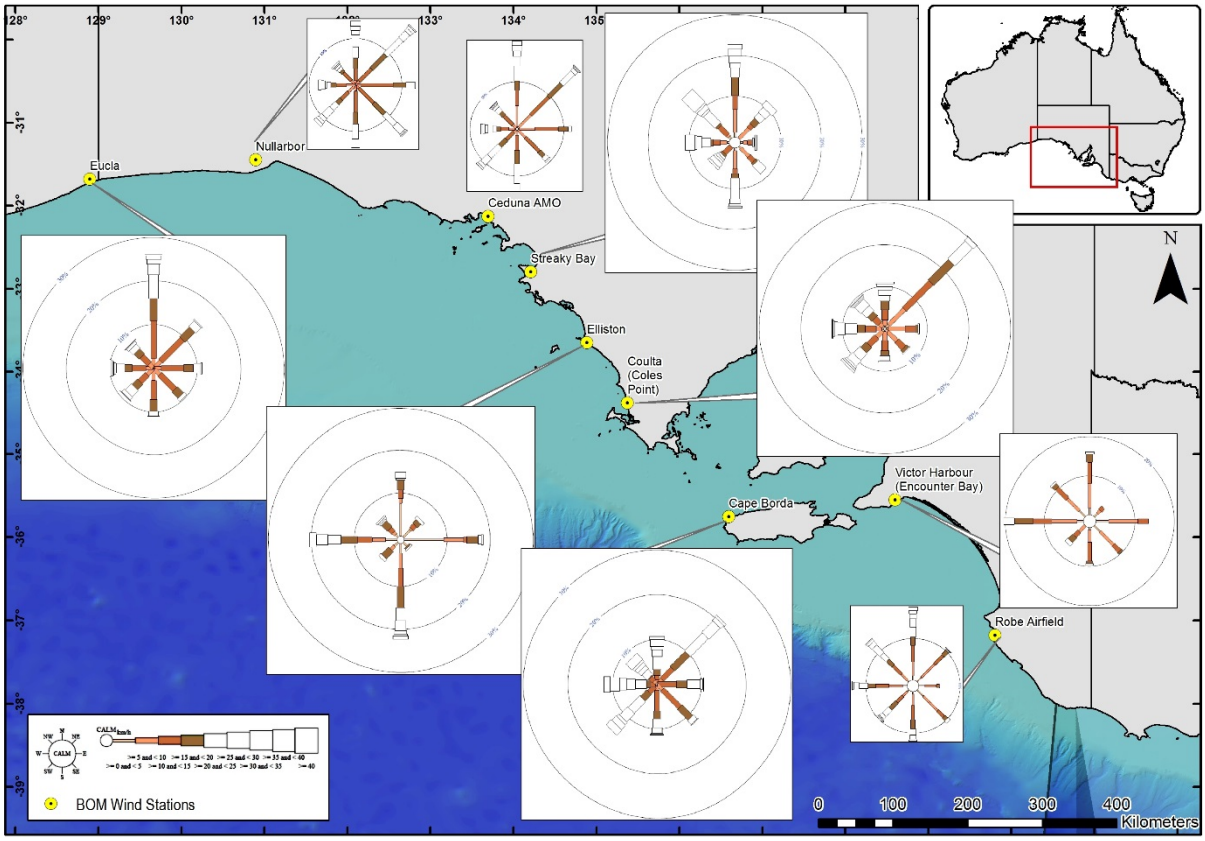

Figure 157: Average winds measured by coastal weather station for July-August-September 2014.

Predominant regional currents

Water movement along the Southern Australian margin is dominated by several currents both at the surface and within the water column. These are briefly described below and shown in Figure 158.

The Flinders Current

Is a proposed western boundary current which runs from east to west at depths of between 500–600 m. With amplitudes of 20 cm/s and 8-14 cm/s in winter and summer respectively, this flow is known as the Flinders Current (FC, Figure 158).

During winter, easterly winds that increase in amplitude with latitude give rise to an equatorward Sverdrup transport in the Southern Ocean which in turn is directed to the west along Australia's southern shelves. (Bye 1968). During summer, winds blow to the west within the GAB and the Sverdrup transport and thus the FC should generally be larger than in winter. Evidence and modelling of the current is presented in Schodlok & Tomczak (1997), Middleton & Bye (2007) and Richardson (2012)

A deep (5000 m) transect of Conductivity/Temperature/Depth (CTD) data taken by at 120°E indicates deep upwelling (1000–500 m) that supports the existence of the FC. The limited CTD, Accosutic Doppler Current Profiler (ADCP) data and numerical model output indicates that it may well be intermittent in space and time and at times non-existent. However, analysis of water mass properties (Temperature T, Salinity S, and stable isotopes) show that the deep (600 m depth) water off the western shelf of Tasmania is directly related to that upwelled onto the shelf (100 m) off Kangaroo Island and also to that found on the slope of the western GAB (Richardson, 2012).

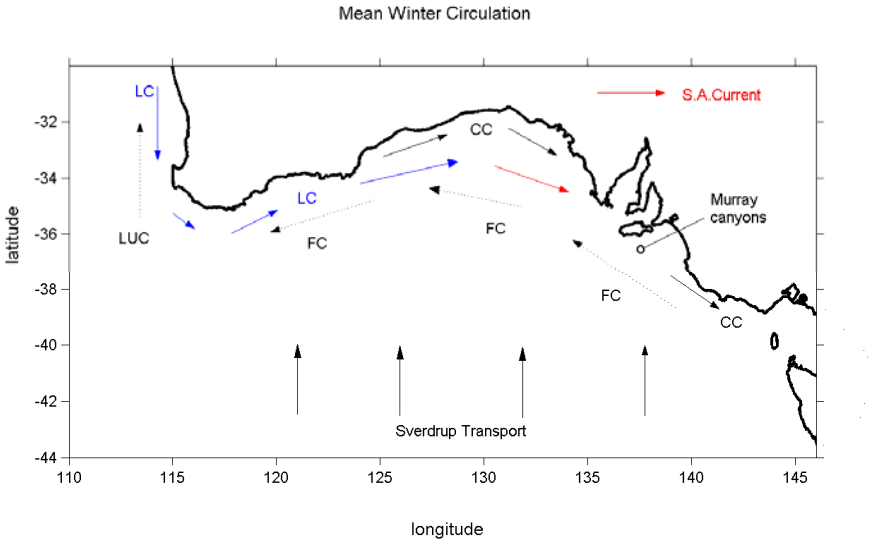

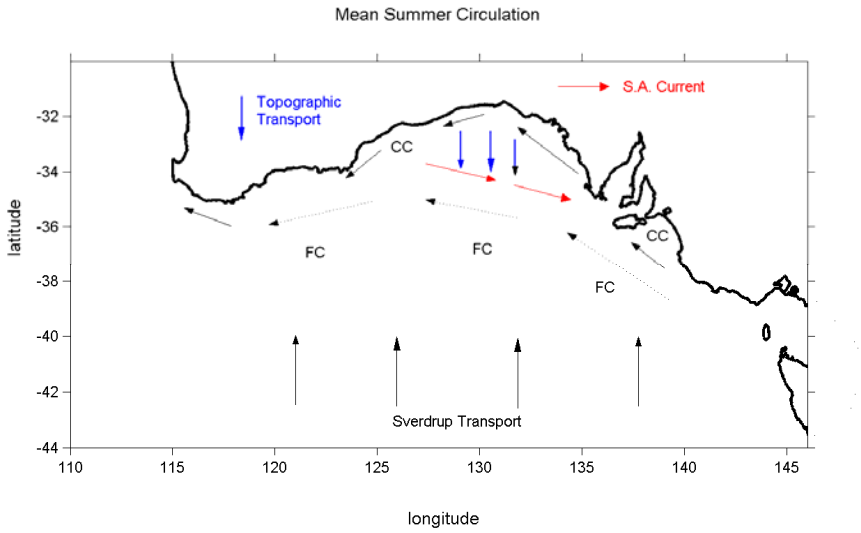

Figure 158: Upper Panel: A schematic of some key circulation features for winter, including the Leeuwin Current (LC), Leeuwin Under-Current (LUC), Flinders Current (FC), shelf-edge South Australian Current (SAC) and coastal currents (CC). Water is downwelled throughout and a dense salty outflow from the Gulfs. Lower Panel: Summertime circulation and upwelling occurs off Kangaroo Is and the Bonney Coast. Shelf edge downwelling may occur in the western Bight.

The Leeuwin Current

During winter, the Leeuwin Current (LC) penetrates the western GAB at speeds up to 1 m/s (Figure 158). The relatively warm water associated with the LC can extend as far as the eastern GAB as indicated by the sea-surface temperature (SST) image shown in Figure 159. During summer, the penetration of the LC into the GAB is much weaker or non-existent.

Coastal Current

Over the shelf, the LC reinforces the (winter) wind driven, geostrophic coastal current (CC) that is directed to the east with amplitudes of 10–50 cm/s (Figure 158). The CCs is not steady and the changes in wind speed and direction give rise to variations in sea level and an alongshore current called Coastal-Trapped Waves (CTWs). During the passage of cold fronts, CTW velocities in the alongshore direction can exceed 1 m/s (Middleton & Bye, 2007). Similarly, under calm conditions, the CCs can be quite small.

Mesoscale Eddies

An additional feature of the circulation in the GAB is the presence of mesoscale eddies during both winter and summer. Surface eddy velocities are of the order 25 to 50 cm/s. These velocities may penetrate to depth and effect local cross-shelf exchange including both upwelling and downwelling. Such eddies can result from baroclinic instability and/or vortex stretching/squashing and, like the weather, are generally difficult to predict with numerical ocean models. However, there does seem to be some coherence in the eddy field as indicated by the meso-scale anomalies in sea-surface height that persist in space and over several months.

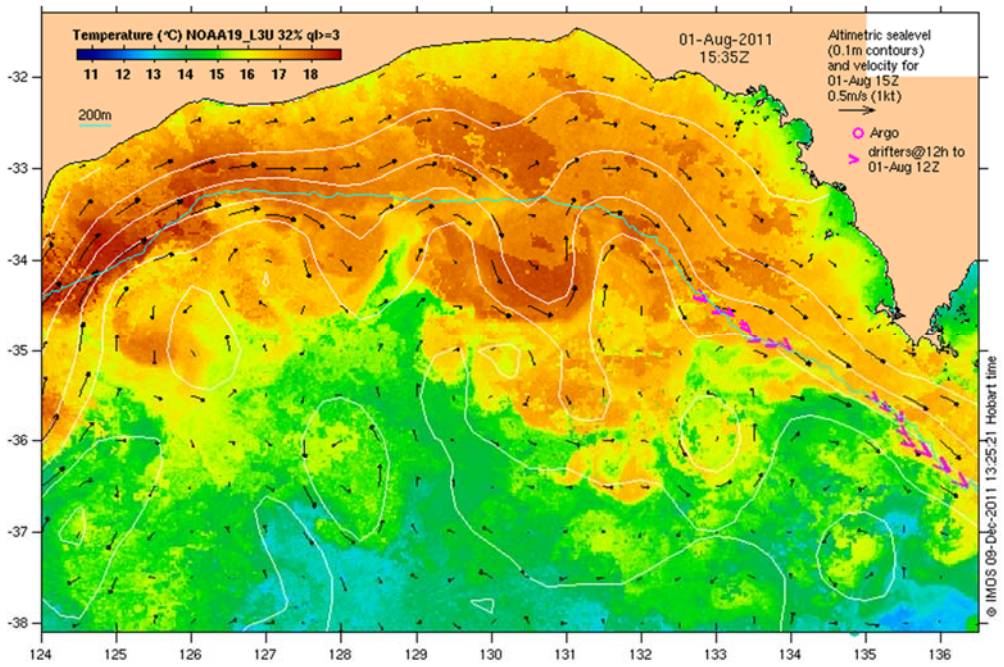

Figure 159: An SST image for August 2011. Warm water associated with the Leeuwin Current enters the western GAB: temperature scale shown. Surface sea level height (altimeter data) is indicated by the white contours. The surface geostrophic velocities are also shown with a legend arrow of 0.5 m/s. The magenta arrow heads denote surface drifter positions at 12h intervals. The cyan line denotes the 200 m isobath and shelf edge. (Source: oceancurrent.imos.org.au).

Other oceanographic processes

Upwelling

The summertime upwelling off Kangaroo Island and the Eyre Peninsula can be largely forced by winds. On the 26th January 2012, a high-pressure system dominated the GAB, with winds directed to the northwest for the Eyre Peninsula to Bonney Coast regions.

The wind-forced upwelling brings cold, nutrient-rich water from depths of 200–400 m (Figure 160) and up onto the shelf (Kaempf et al., 2004; Middleton and Bye, 2007; Kaempf, 2010; Richardson, 2012). The upwelled water resides near the bottom between Kangaroo Island and the southern Eyre Peninsula as a nutrient-rich cold pool that then acts to feed subsequent upwelling events and lead to phytoplankton growth for the region (McClatchie et al., 2006; Van Ruth et al., 2010a, b). Accordingly, higher levels of chlorophyll (~phytoplankton biomass) are found off the Bonney Coast and the Eyre Peninsula.

Upwelling is likely forced by winds in the GAB has also been observed in the far-western GAB and for the narrow shelf region between Esperance and Cape Leeuwin (van Hazel, 2001). Notably, no strong evidence of upwelling is found in the mid or western GAB.

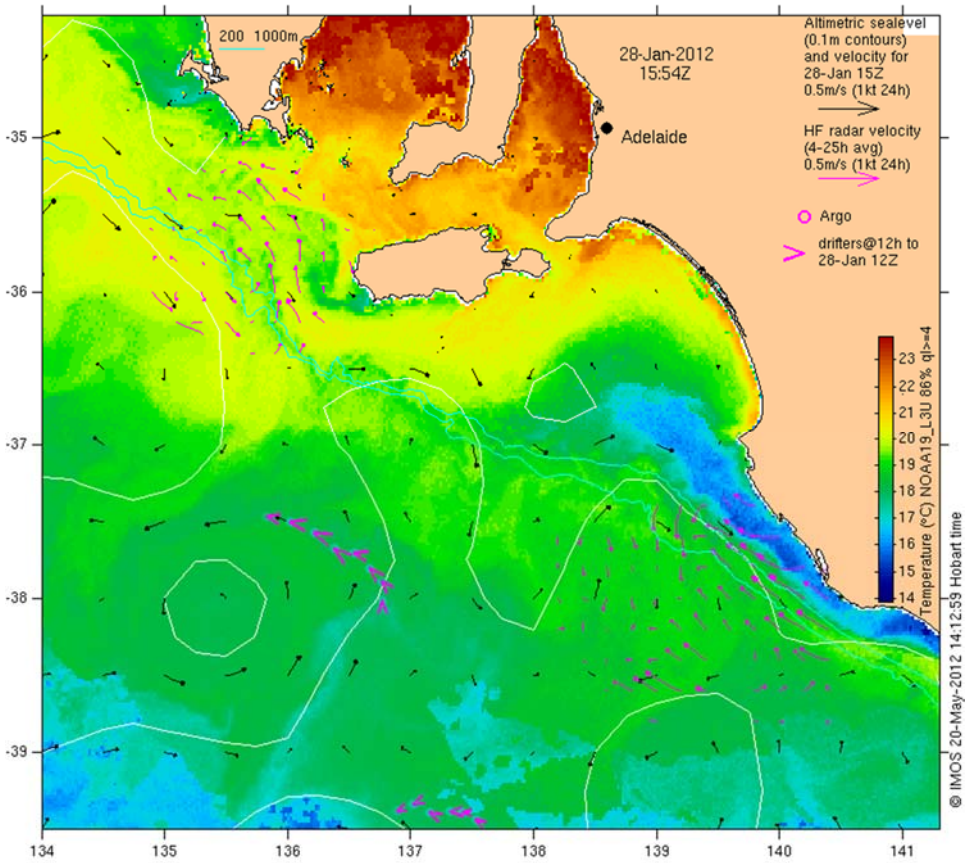

Figure 160: A SST image for 28th January 2012. Warm (23 °C) water associated with heating in the shallow Gulfs is shown along with cold (14-18 °C) upwelled water off the Bonney Coast, Kangaroo Island and the Eyre Peninsula: temperature scale shown. Surface sea level height (altimeter data) is indicated by the white contours. The surface geostrophic velocities are also shown with a legend arrow of 0.5 m/s. The magenta lines correspond to HF RADAR daily-averaged currents with a legend arrow of 0.5 m/s shown. The magenta arrows denote surface drifter positions. The cyan line denotes the 200 m isobath and shelf edge. (Source oceancurrent.imos.org.au).

Downwelling

During winter, evaporation exceeds precipitation for the coastal regions and, combined with surface cooling, leads to the formation of relatively cold, salty water along the coastal regions of the shelf and also in the gulfs. The winds during winter also generally favour downwelling with the result that the dense coastal water is pushed down along the deeper offshore regions of the shelf and slope (Bye, 1968; Rochford, 1986; Middleton and Bye, 2007).

During summer in the mid-GAB, the cross-shelf exchange is dominated by downwelling. The reason for this appears to be related to the summer circulation on the wide shelf region in the mid-GAB.

Within the wide sloping shelf of the mid-GAB, anticyclonic (anti-clockwise) winds drive southward topographic Sverdrup transport (Figure 158: Herzfeld & Tomczak, 1999) and, in conjunction with the westward coastal currents, gives rise to an anticyclonic circulation within the mid-GAB. The southward topographic transport converges at the shelf break with the northward deep ocean Sverdrup transport and leads to downwelling to depths of 250 m.

El-Nino - La Nina Effects (ENSO)

ENSO events occur with a 4 to 7 year period, originate in the Pacific and likely effect the circulation, upwelling and downwelling of the GAB (Middleton & Bye, 2007). For the Australian region, the depressed shelf sea level and raised thermocline that arise in the west Pacific Ocean during an El Nino event, is transmitted around Papua and New Guinea and down the West Australian shelf as a type of slope-trapped wave.

Observations show that the wintertime LC and mean shelf currents are substantially reduced during the onset of strong El Nino events. In addition, CTD data from the Kangaroo Island region indicates that during an El Nino summer, the thermocline may also be raised by 170 m so that wind-forced upwelling can increase the level of nutrients and cold water on the shelf. During strong La Nina events the reverse may hold with the thermocline depressed and westward shelf currents enhanced.

Surface Waves and Tides

The GAB has a mixed wind wave/swell environment in which at any location the sea-state rapidly 'deteriorates' during the passage of fronts and low-pressure systems, and then gradually 'moderates' as anticyclonic conditions return. The wave climate is mildest in February (Figure 161; upper panel) and wildest in September (Figure 161; lower panel).

Statistics of the wave climatology are presented in Table 41 for the mid-GAB in February and July (Caires et al., 2005; Middleton & Bye, 2007; Hemer & Griffin, 2010). The significant wave height (H_s), wave speed (c), wavelength (λ) and the three velocities – the surface orbital velocity (U_0), the bottom (50 m) orbital velocity (U_b) and the Stokes surface drift velocity (U_d) – have been calculated from deep-water gravity wave theory. The wave drift velocity would occur predominately in an onshore direction, and the mean speed of about 0.15 m/s indicates that over a month, surface biota would be advected shorewards by a distance of about 390 km – a scale which exceeds the shelf width. The possible importance of this wave drift, which is in addition to the downwelling flows discussed above, is not yet known. Caires et al., (2005) also indicate that the wave height will exceed 3 m for 30-60 days of the year and 6 m for 0–10 days of the year. The bottom orbital velocities on the open continental shelf will therefore exceed 0.2 m/s and 0.4 m/s and may lead to a significant sediment re-suspension.

These results are augmented by the observations made by Wood and Terray (2005) for the April-September period of 2004 just south of Portland (water depth 1395 m). They found the waves to have a significant height of 3.7 m, a period of 13 seconds and to be directed from the southwest. Wave heights exceeded 8 m for 1.3% of the time, and 5 m for 17% of the time. Statistics of the long-term buoy data and from satellite altimetry are given by Hemer and Griffin (2101).

Tidal currents on the shelf and within the GAB are generally small (< 10 cm/s) and do not appear strong enough to induce any internal tides of any significance (Hahn, 1986; Middleton & Bye, 2007).

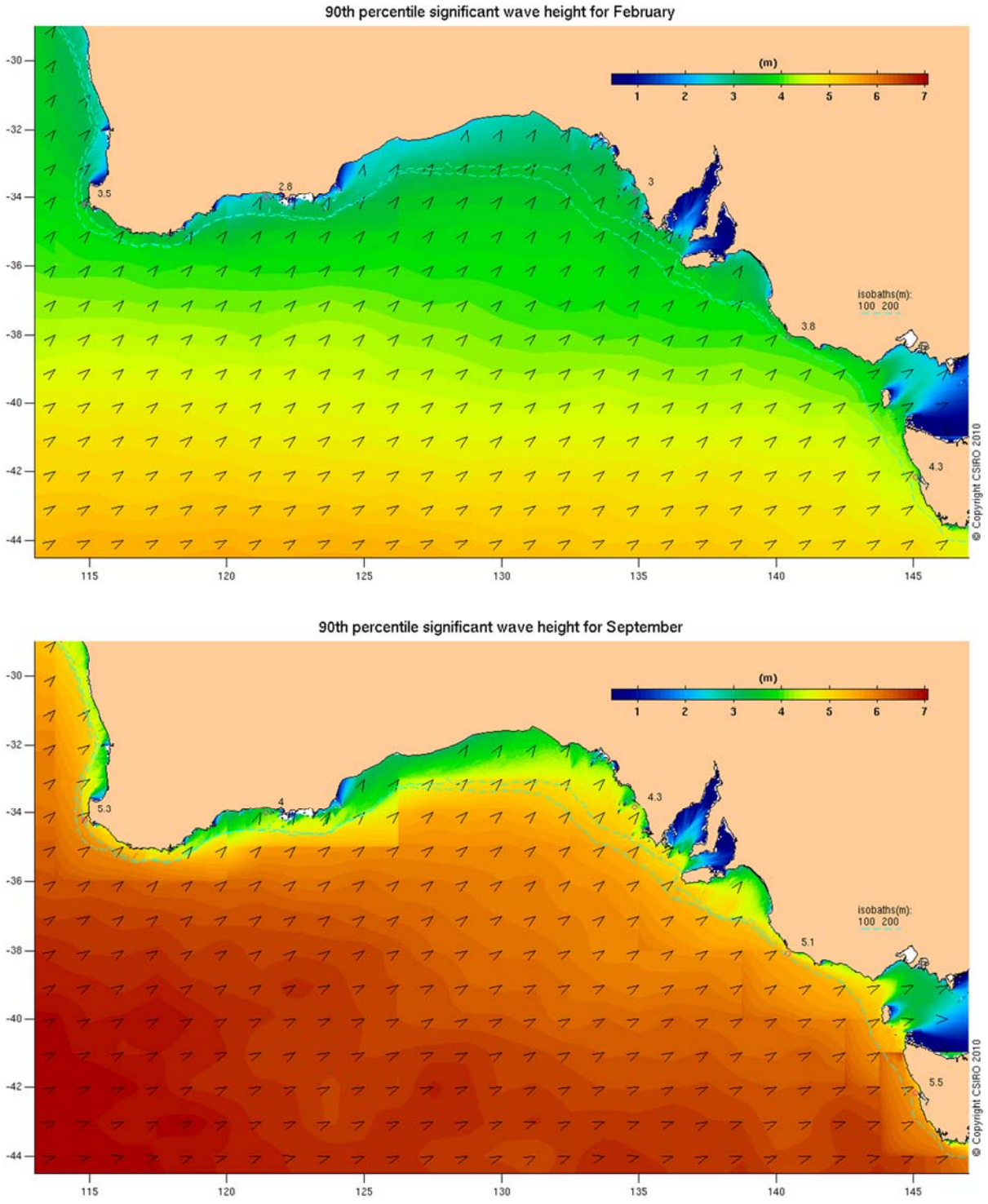

Figure 161: Climatological 90th percentile wave height (see key) and direction (arrow heads) for February (upper panel) and September (lower panel), from Hemer & Griffin (2010). For other months and percentiles, see http://www.marine.csiro.au/~griffin/ORE/wave_height/index.html.

Table 41: Wave climatology for the mid-Bight as inferred from Caires et al., (2005) including the significant wave height HS, period T, phase speed c, wavelength λ. The surface and bottom water velocities are denoted by Uo and Ub the (Stokes) drift velocity by Ud. The standard deviations (σ) of HS and T are also presented: units metres. Note the significant wave height is the average height of the top 33% of wave maxima averaged over a month.

Month	H_S (m) σ (m)	T (s) σ (s)	c (m/s)	λ (m)	U_o (m/s)	U_b (m/s)	U_d (m/s)
Feb	2.25 0.45	7.5 1.8	11.7	88	1.9	0.05	0.16
July	2.75 0.90	9 1.8	14	126	2.0	0.16	0.14

Oceanographic modelling of asphaltite and tarball strandings in Great Australian Bight

Rationale and hypothesis

Stranding locations of tarballs (waxy bitumens) and asphaltites, when used in conjunction with data from oceanographic, geological and weathering models, could lead to the definition of their possible origin points within the GAB and beyond. The Great Australian Bight Research Program Oceanography Theme has produced several oceanographic models of the GAB region that have been validated against available data (and each other).

It is expected that the models will have sufficient skill to allow tracking of both tarballs (positively buoyant) and asphaltites (quasi-buoyant) within the GAB, from proposed origin points in the GAB using a forward modelling approach; and from shoreline stranding locations using a hindcast/backtrack modelling approach.

Whilst it is unlikely that oceanographic modelling will permit definitive determination of the origin locations of the asphaltites and tarballs, probability transition matrices in combination with detailed geochemical fingerprinting, seismic data interpretation and our knowledge of the geology the sedimentary basins along Australia's southern margin will enable hypothesis and conceptual model testing.

Hypothesis to be tested:

Tarball and asphaltite stranding locations or potential origin points can be predicted using oceanographic models with geologically rational offshore seeding locations or stranding locations.

1. Oceanographic back-track modelling of coastal bitumen strandings based on their spatial distribution may be used to identify regions of interest within the GAB that may represent sites of hydrocarbon seepage.

2. Forward modelling through seeding particles from potential seepage sites may show a reasonable level of agreement with the observed spatial distribution of coastal bitumen strandings (forward modelling bitumen from potential offshore seep origins to stranding locations).

What the models cannot do:

1. Models may not show the actual bitumen path at a particular point in time. The oceanographic model outcomes presented herein are for testing scenarios using the information provided from the annual beach surveys. For example modelled years may not overlap with the beach surveys (e.g. using 2014–2016 survey data in 2009–2012 SHOC models)

2. Models will not directly identify points of seepage. There is a need to analyse the resulting movement of particles for potential areas of overlap, and then cross-reference this information with the geology of the region to assess the potential for seepage.

Oceanographic models

A detailed description of the oceanographic models used during the Great Australian Bight Research Program (GABRP) can be found in Middleton et al., (2017). However for context a summary of these models and their operation is included below.

The oceanographic models used to model the behavior of asphaltites and tarballs are based on global circulation models that are estimates of the three-dimensional time-varying ocean (its temperature, salinity, sea-level and three components of velocity) over long periods of time. These models have a relatively coarse resolution in both space and time. Errors in the fields of temperature (T) and salinity (S) in the global models can, for example, lead to errors in the regional models. However, no alternatives exist if realistic simulations are required to understand inter-annual variability due to large-scale processes such as El Nino, Indian Ocean Dipole or Southern Annular Mode. Moreover, differences in the topography and grid size of the global and regional models can also lead to errors in the latter. The global models are briefly described below, followed by details of the regional models used for the GAB.

Global Models

The global model used in this study is BRAN2015. Importantly, this model is a data-assimilating model, meaning it uses all available observations in order to be correct (i.e. just like a weather forecast). Details of the BRAN2015 model can be found in Oke et al., (2013a, b). This model originated from the Bluelink ReANalysis model (BRAN3.5; http://www.cmar.csiro.au/staff/oke/BRAN.htm). BRAN3.5 is a 1992 to mid-2012 integration of OFAM2 that assimilates ocean observations in order to be more 'correct' on a point-by-point basis than a non-assimilating integration, but at some cost in terms of dynamical self-consistency.

The following changes were made to BRAN3.5 so as to improve skill and the product called BRAN2015 that covers the period 1st April 1992 to July 2015. BRAN2015 was made available in December 2015. Whilst the observations used for assimilation in BRAN3.5 and BRAN2015 remain the same in the Australian region, the latter model uses the OFAM3 (Ocean Forecasting Australia Model) and also has improvements in the data assimilation system, the initialisation method and atmospheric forcing.

OFAM3 (Oke et al., 2013a) is the third (and latest) major revision of the Ocean Forecasting Australia Model (OFAM) developed by CSIRO as part of the CSIRO-BoM-RAN Bluelink project. OFAM3 is the

first version of OFAM to be (almost) fully global – its 0.1 x 0.1° horizontal grid extends from 75°N to 75°S, so that the model is mesoscale eddy resolving for all the western boundary currents and other regions such as the sub-Antarctic frontal region in the Southern Ocean.

Some of the main improvements and changes implemented through using the BRAN 2015 model versus the BRAN3.5 model are:

- Long integration of OFAM3 (see above) like other global models such as OFAM3-JRA55
- Stronger (14-day e-folding timescale) restoring of surface salinity to CARS climatology than OFAM3-JRA55, whereas BRAN3.5 used no salinity restoring. Both systems used no restoring of SST.
- BRAN3.5 extended from 1992 to mid-2012, while the new BRAN2015 extends from April 1st 2009 to mid-2015 covering the total period of interest for this project.
- Better correlation of modelled versus observed temperature data (this correction should lead to an improved comparison with the data).

Regional Models

Sparse Hydrodynamic Ocean Code (SHOC):

SHOC is a hydrodynamic model developed by CSIRO (Herzfeld, 2006) (http://www.emg.cmar.csiro.au/www/en/emg/software/EMS/hydrodynamics.html). It has been applied to a number of regions (http://www.emg.cmar.csiro.au/www/en/emg/Publications.html) and contains options for many of the advective and mixing schemes that have been developed and adopted elsewhere. It also incorporates a highly irregular grid that can be used to focus resolution where it is most desired, and optimise the orientation of open boundaries with respect to the topography. It was considered for use with this project. However, due to the improved skill and enhancements made to the BRAN2015 model, the SHOC model was not adopted for this project and with a regional BRAN2015 model being used instead.

Regional Ocean Modelling System (ROMS):

ROMS is an open-source hydrodynamic model (myroms.org) that is used by over 3,800 oceanographers world-wide and is subject to many hundreds of applications many of which are peer reviewed. It also contains options for many advective and mixing schemes and the presence of land cells make no difference to computational time. It is the model adopted by SARDI for all projects (e.g., Middleton et al., 2014a; 2014b; McLeay et al., 2016).

The model domains used are illustrated in Figure 162 and Figure 163. The sites of the mooring data and sea level data (Thevenard) are also indicated and the data from these sites were used in preliminary theme 1 model validations and comparative studies. The ROMS and SHOC models implemented here have quite distinct domains and grids and are respectively embedded in different global ocean models: BRAN2015 (Bluelink Re-Analysis, i.e. a model that assimilates data). ROMS and SHOC models also use different topographies, mixing schemes and surface meteorology, as indicated in Table 42 where a summary of model details is given. Agreement (or the lack thereof) between such distinct models will provide one measure of skill.

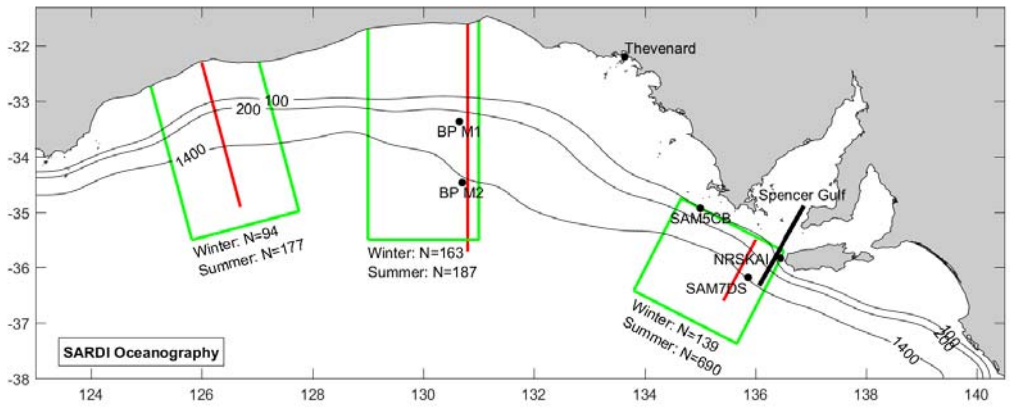

Figure 162: The ROMS model domain ("SAM") used in this study. The 100 m, 200 m and 1400 m isobaths are shown. The mooring locations of SAM5CB (Coffin Bay), NRSKAI (Kangaroo island), SAM7DS (deep 600 m mooring) and the BP moorings BPM1 (shelf edge) and BPM2 (shelf slope) are shown. The thick straight black line indicates the repeat SAIMOS CTD line. The red lines denote the location of cross-sectional (seasonal averaged) model results. The green boxes denote the domains for which all available temperature data is obtained so as to compare with the (red line) cross section model results. The number N of temperature data casts for each green box is indicated for summer and winter.

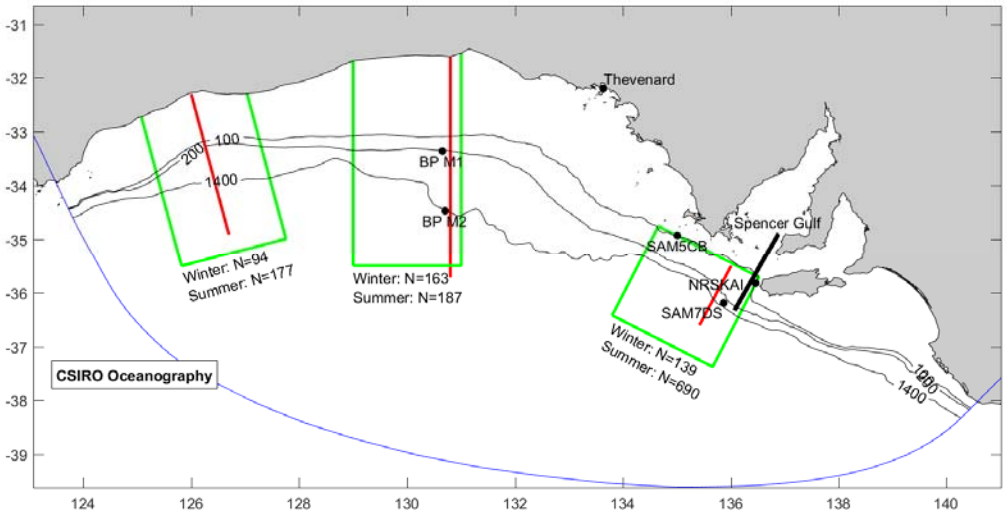

Figure 163: As in Figure 162 but for the BRAN2015 model domain used by CSIRO in this study. The thin blue line demarcates the model open boundary.

Table 42: Parameters and forcing components used for the ROMS and BRAN models in the study. The acronyms, abbreviations and references used are indicated below.

Numerical component	ROMS V2	BRAN
Simulation ID number(s)	o1236173/o1239579	BRAN2015
Simulation interval	January 2011 – December 2014	January 1992-Present
Name of grid	SAM	GAB5
Size of grid	163 x 350 horizontal	430 x 199 horizontal

Numerical component	ROMS V2	BRAN
	30 vertical	55 vertical – 0.5m at surface
Horizontal grid cell size	0.04° (approx. 4 km)	0.1 deg x 0.1deg x 51 layers (constant thickness, ranging from 5m at surface to thick at depth).
Horizontal coordinate system	Uniform	Geographic rectangular (false pole)
Vertical coordinate system	Terrain-following stretched	51 layers (constant thickness, ranging from 5m at surface to thick at depth).
Bottom drag formulation	Quadratic (2.25×10^{-3})	Quadratic (variable roughness)
Vertical mixing parameterisation	Mellor-Yamada 2.5	Harcourt (2013,2015)
Horizontal eddy viscosity coefficient	5 m^2/s	150 m^2s^{-1} + Smagorinsky (c=0.1)
Horizontal mixing coefficient for temperature and salt	2 m^2/s	Smagorinsky (c=0.1)
Bathymetric data set	Geosciences Australia 2009 0.005°. Minimal smoothing	Gebco 2008 data merged with GA around Australia. Many straits manually edited using a GUI
Initial conditions (T, S, u, v, U, V)	BRAN2015 (CSIRO global model)	BRAN2015 (CSIRO global model)
Open boundary nesting: T & S source Width of nudging layer Time scale at boundary Time scale at interior	 BRAN2015/10 days 0.4° (~40 km) 1/3 days 1/30 days	 BRAN2015 0 n/a n/a
Open boundary condition: source Variable/Type Variable/Type Variable/Type	 BRAN 2015 Sea level / U & V / Schchepetkin u & v / Orlanski (modified)	Herzfeld & Andrewartha (2012) BRAN2015 Sea level unconstrained u,v Dirichlet U,V integrals of u,v
Surface heat flux correction data source/time scale	NCSS (SST)/monthly (adjusts heat flux so model tends towards observations)	None
Surface momentum and heat fluxes	ECMWF	ACCESS-R
Surface pressure forcing	No	Yes
Bulk formulation for surface fluxes Y/N	No	Yes (Kondo 1975)
Global tidal model	TPXO 8.1	None

Model parameterisations

Scenario 1 – Comparison of winter and summer offshore seeded particle trajectories using currents only

Model used/mode:

ROMS forward tracks

Hypothesis tested:

Hypothesis #2. Seeding particles from potential seepage sites within the GAB region may show a reasonable level of agreement with the observed spatial distribution of coastal bitumen strandings (forward modelling bitumen from potential offshore seep origins to stranding locations).

Purpose:

To determine if general patterns of stranding of asphaltites and tarballs can be mimicked to a reasonable level of agreement based on particular hypothetical release points on surface currents alone.

Scenario details:

- Seed the model from the selected offshore potential origin points (Figure 164 and Table 43)
- Only horizontal component active in the ROMS model since the particles are simulated as near surface or surface drifters only.
- No Stokes drift or windage applied in model to surface drifters.
- Release points over 2 X 2 model cells of 8 X 8 km in the horizontal (patch) with centroid being as close to potential origin point as possible.
- Each patch will have 4 particles and be seeded at three 10-day intervals and all tracked for 90 days following release.
- Two seasonal periods tested, winter and summer.
- For summer, the three dates of deployment (seeding) at every site (or patch) 2nd, 12th and 22nd January for each of the 4 years (2011, 2012, 2013 and 2014). The particles are all tracked for 90 days following seeding (release).
- For winter, the three dates of deployment (seeding) at every site (or patch) and depth noted above are 2nd, 12th and 22nd July for each of the 4 years (2011, 2012, 2013 and 2014). The particles are all tracked for 90 days following seeding (release) and so effectively cover a summer and winter season.

Scenario 2 – Offshore seeded particle trajectories using currents and wave movement

Model used/mode:

BRAN2015 forward tracks

Hypothesis tested:

Hypothesis #2. Seeding particles from potential seepage sites within the GAB region may show a reasonable level of agreement with the observed spatial distribution of coastal bitumen strandings (forward modelling bitumen from potential offshore seep origins to stranding locations).

Purpose:

To determine if general patterns of stranding of asphaltites and tarballs can be mimicked to a reasonable level of agreement based on particular hypothetical release points, using both surface currents and Stokes drift (the effect of waves on particles).

Scenario details:

- Seed the model from the selected offshore potential origin points (Figure 164 and Table 43)
- Particles are simulated as near-surface or surface drifters only in BRAN2015 model.
- Stokes drift (1.5% of wind) applied in model to surface drifters.
- Release points over 2 X 2 model cells of 8 X 8 km in the horizontal (patch) with centroid being as close to potential origin point as possible.
- Each patch will have 12 particles seeded at each release time
- Three model iterations-
    - Scenario 2.1 – 1-month trajectory models with seeding occurring on 1 day of each month
    - Scenario 2.2 – 2-month trajectory models starting on day 15 of each month
    - Scenario 2.3 – 3-month trajectory models starting on day 10 of each month
- Time period for models 01/01/2013-30/11/2016

Table 43: Offshore seeding locations for the forward track oceanographic models.

Seed Locations offshore sites	Latitude WGS84	Longitude WGS84	South WGS84 Zone 52S	East WGS84 Zone 52S	Water depth (m)
00 Eyre Canyon GA Dregded Canyon	-33.67199744	128.7578071	6274185.017	477548.3848	2203
01 BP EPP38 west canyon	-34.44770173	129.769078	6187933.711	570648.6881	2646
02 East Canyon	-35.71119552	133.2954392	6039570.232	888661.1754	2213
03 Chevron EPP45 Canyon	-35.70405714	132.881413	6041926.344	851211.1633	2599
04 Chevron EPP45 Pockmarks	-35.41138344	132.5102171	6075672.317	818767.7542	1798
05 Chevron EPP45 West Canyon	-35.50418241	132.1318828	6066531.062	784071.8434	2463
06 BP EPP39/40 border Canyon	-35.03304914	130.9040809	6121634.778	673691.6364	2405
07 Murphy Oil EPP43 GA Cored Canyon	-33.54112708	130.0688901	6288209.533	599239.5408	876
08 Leeuwin Current	-34.08804075	126.5494465	6225371.283	273904.6028	3303
09 Ceduna Basin East shelf break	-34.9162	133.65436	6126349.31	925312.9791	365
10 S12-2 Ceduna Basin North Shelf Break	-33.56839	131.4008	6283115.91	722849.2286	431
11 S12-2 Ceduna Basin North East Shelf Break	-34.38701	132.77997	6188450.846	847572.9828	298

12 EPP 41 Duntroon Basin West	-35.39363	135.03444	6066542.485	1048338.064	131
13 Murray Basin South Shelf Break	-37.06783898	138.1170295	5858500.487	1311411.548	115
14 Couedic Shelf Break	-36.66469	136.92236	5912961.158	1208632.803	606
15 EPP42 Shelf Break	-35.93283608	135.7685015	6002265.062	1110990.067	164

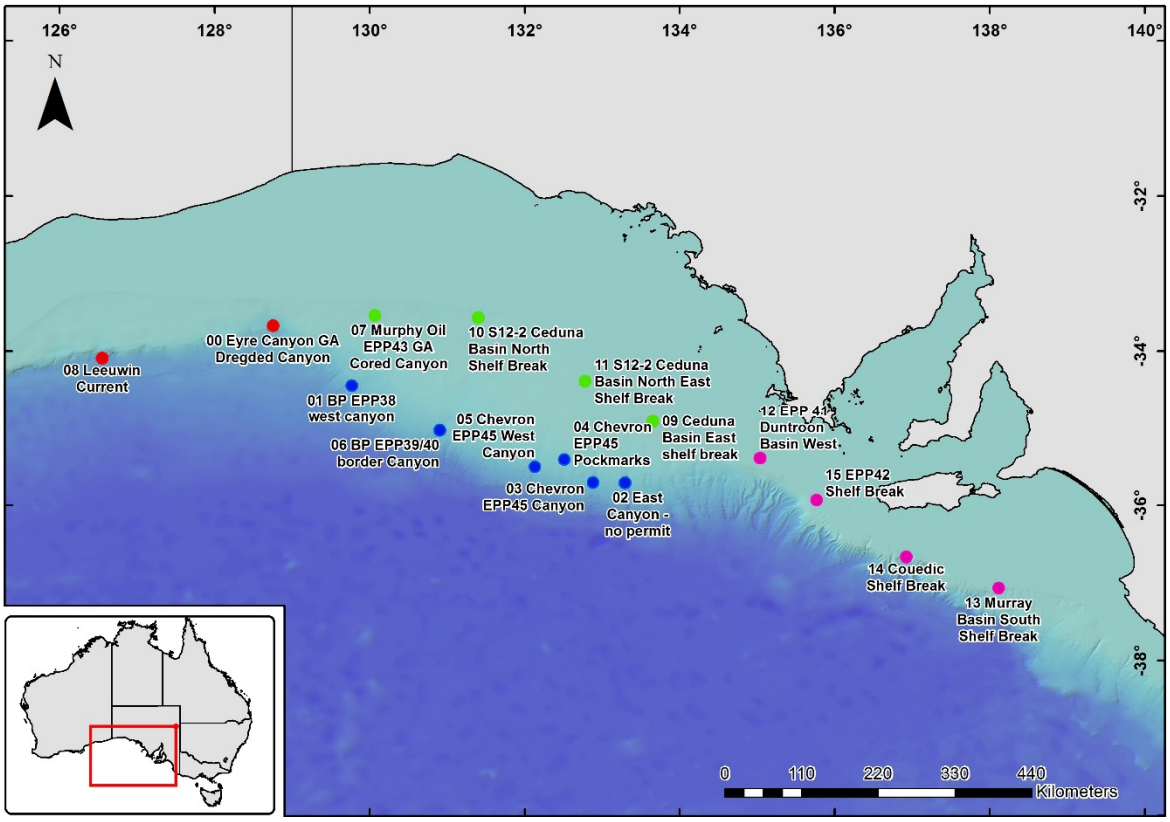

Figure 164: Asphaltite and tarball potential offshore seeding locations used in oceanographic forward models.

Scenario 3 - Back track trajectories from beach seeding locations using currents and wave movement

Model used:

Bran 2015 Backtracks

Hypothesis tested:

Hypothesis #1 Oceanographic modelling of coastal bitumen strandings based on their spatial distribution may be used to identify regions of interest within the GAB which may represent sites of hydrocarbon seepage (backtracking bitumen through currents).

Purpose:

To determine if it is possible to use ten beaches across the sudy area where there were strandings of asphaltites and tarballs to identify common potential origin locations

Scenario details:

- Seed the model close to beach locations (within model capabilities)
- Particles are simulated as near surface or surface drifters only in BRAN2015 model.
- Stokes drift (1.5% of wind) applied in model to surface drifters.
- Release points over 2 X 2 model cells of 8 X 8 km in the horizontal (patch) with centroid being as close to potential origin point as possible.
- Each patch will have 4 particles seeded at each release time
- 3-month trajectory models starting on the last day of each 3-month period (March, June, September, December)
- Time period for models 01/01/2013-30/11/2016

Table 44: Beaches used as seeding locations for backtrack models.

Beach	LatY	LngX
Cactus Beach	-32.0739	132.9761
Coffin Bay	-34.66	135.49
Elliston	-33.635	134.8753
Eve's / Evan's Cove	-37.1839	139.7462
Eyre Well	-31.4639	131.1422
Fowlers Bay West	-31.9928	132.4375
Geltwood Beach	-37.6601	140.2235
Tractor Beach	-32.8696	134.1125
Waitpinga Beach	-35.6362	138.5061
West Bay	-35.8858	136.5512

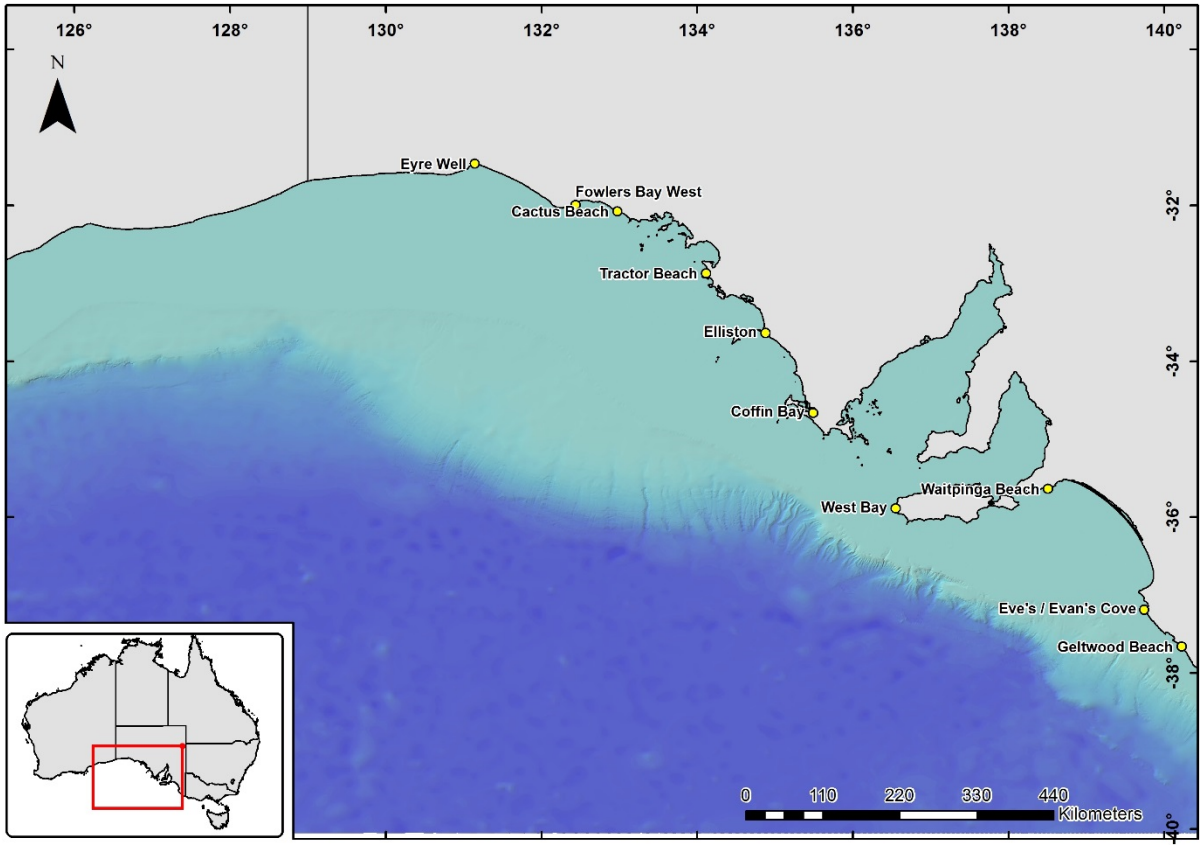

Figure 165: Beach locations used as seeding locations for backtrack models.

Oceanographic modeling results

Scenario 1 - Comparison of winter and summer offshore seeded particle trajectories using currents only

The ROMS modelling of winter and summer offshore seeded particle trajectories showed significant differences between winter and summer trajectories across all of the years modelled.

Summer processes show a number of general trends in the model iterations (Figure 166 to Figure 169) which are summarised below:

a) Offshore surface Ekman transport;
b) Offshore shelf transport in mid-GAB;
c) Shelf/slope blockage with the waters of Spencer Gulf;
d) Weak to absent Leeuwin Current;
e) Eastward SA Current over shelf break from end of Eyre Peninsula eastwards; and
f) Offshore eddies with diameters of 100-200km.

Particle trajectories from the offshore seeding locations from the 1st January – 10th March, 11th January – 20th March and 21st January – 30th March for 2011 (Figure 166), 2012 (Figure 167), 2013 (Figure 168) and 2014 (Figure 169) all show that surface currents alone are unlikely to lead to stranding of materials along the coastline of South Australia. The most probable location where the

particles would encounter the shoreline is along the Limestone Coast and occasionally Kangaroo Island. Another key observation is that the majority of particles released in the model are retained in the deep water meso-scale eddies of the GAB and therefore could be stranded during the winter months. Results between years are similar to each other, with the major differences being in the intensity of the meso-scale eddies in the Southern Ocean and their ability to trap and retain particles.

Winter processes show a number of general trends in the model iterations (Figure 166 to Figure 169) which are summarised below:

a) Onshore surface Ekman transport;
b) Offshore shelf transport;
c) Shelf/slope exchange with the waters of Spencer Gulf;
d) General eastward flow including the Leeuwin Current (LC) (maximum over shelf break); and
e) Offshore eddies with diameters of 100-200km.

Particle trajectories from the offshore seeding locations from the 1st July to 8th September, 11th July to -18th September and 21st July to 28th September for 2011 (Figure 166), 2012 (Figure 167), 2013 (Figure 168) and 2014 (Figure 169) all show that surface currents alone can lead to stranding of materials on the southern end of Eyre Peninsula, Kangaroo Island, and along the Yorke and Fleurieu peninsulas, Coorong and Limestone Coast. The majority of particles released close to the shelf edge are moved east by the Leeuwin Current and lost to the east. However, those particles released in the deep water of the GAB are transported to the west. As with the summer models, some of the particles released into the model can be entrained within deep water mesoscale eddies.

Intra- and inter-annual variation is large, with some model iterations showing particle stranding across much of the Eyre Peninsula, although there are no modelled strandings towards the Head of the Bight, whilst other model iterations have little or no strandings along the Peninsula.

If the results of this current-driven model were considered without the effect of winds and/or waves, materials found on the Eyre Peninsula would be sourced from the west of the central shelf break of the GAB only, whereas materials found on the Limestone Coast could be sourced from anywhere along the margin (consistent with the arrival of Indonesian-sourced bitumen on the beaches of the Limestone Coast). The model is instructive in showing the importance of the regional currents and oceanographic processes and their potential effects on the tarballs and asphaltites. However, the models are insufficient to adequately explain the observed distribution of the asphaltites and tarballs across the region if a local source is assumed, in particular those on the beaches near the Head of the Bight. In addition, this model does not consider the effects of Stokes drift or windage on particles at the water's surface, which would be expected for the buoyant or quasi-buoyant tarball and asphaltites drifters.

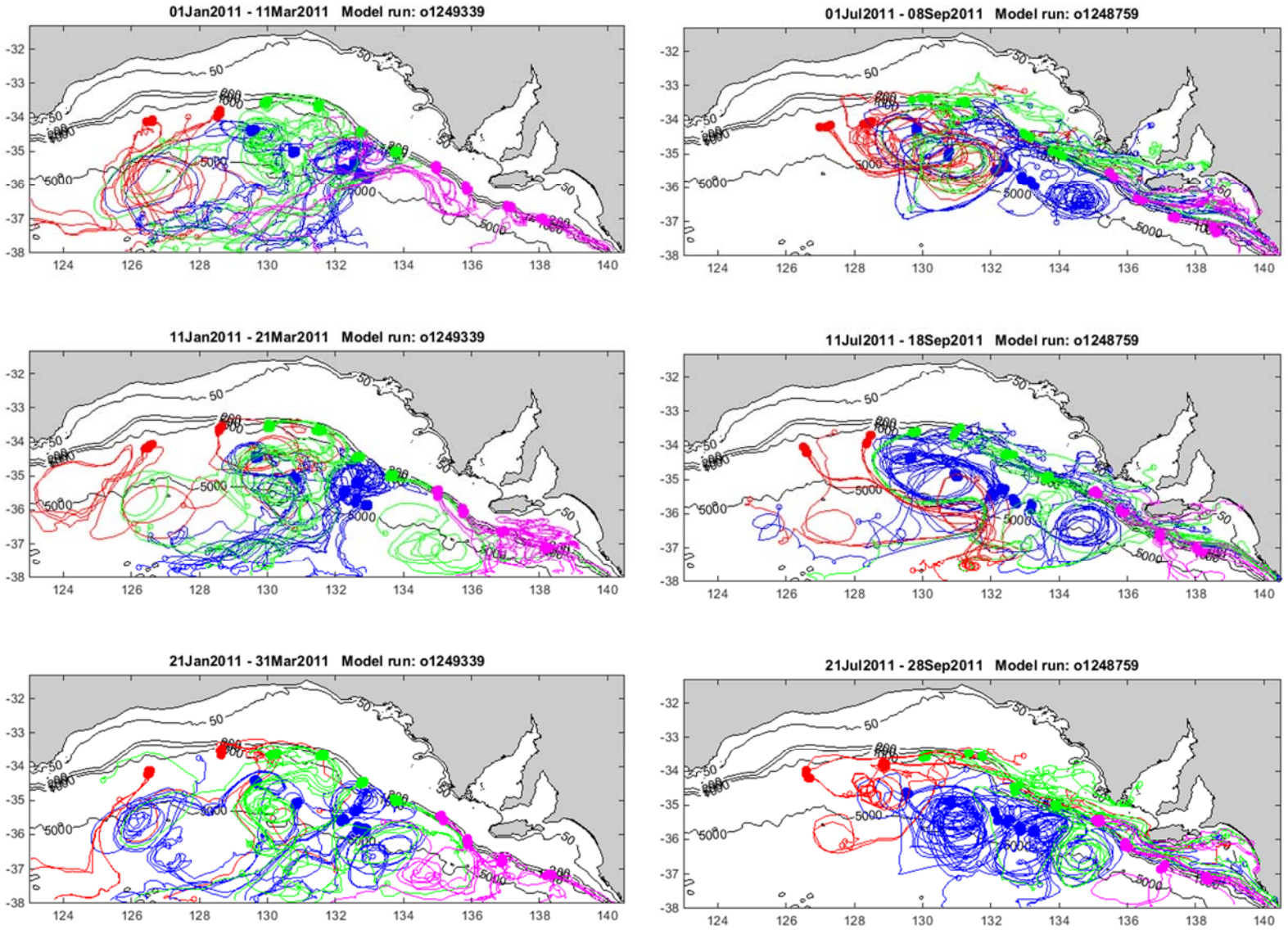

Figure 166: ROMs winter and summer offshore seeded particle trajectories using currents only for 2011.

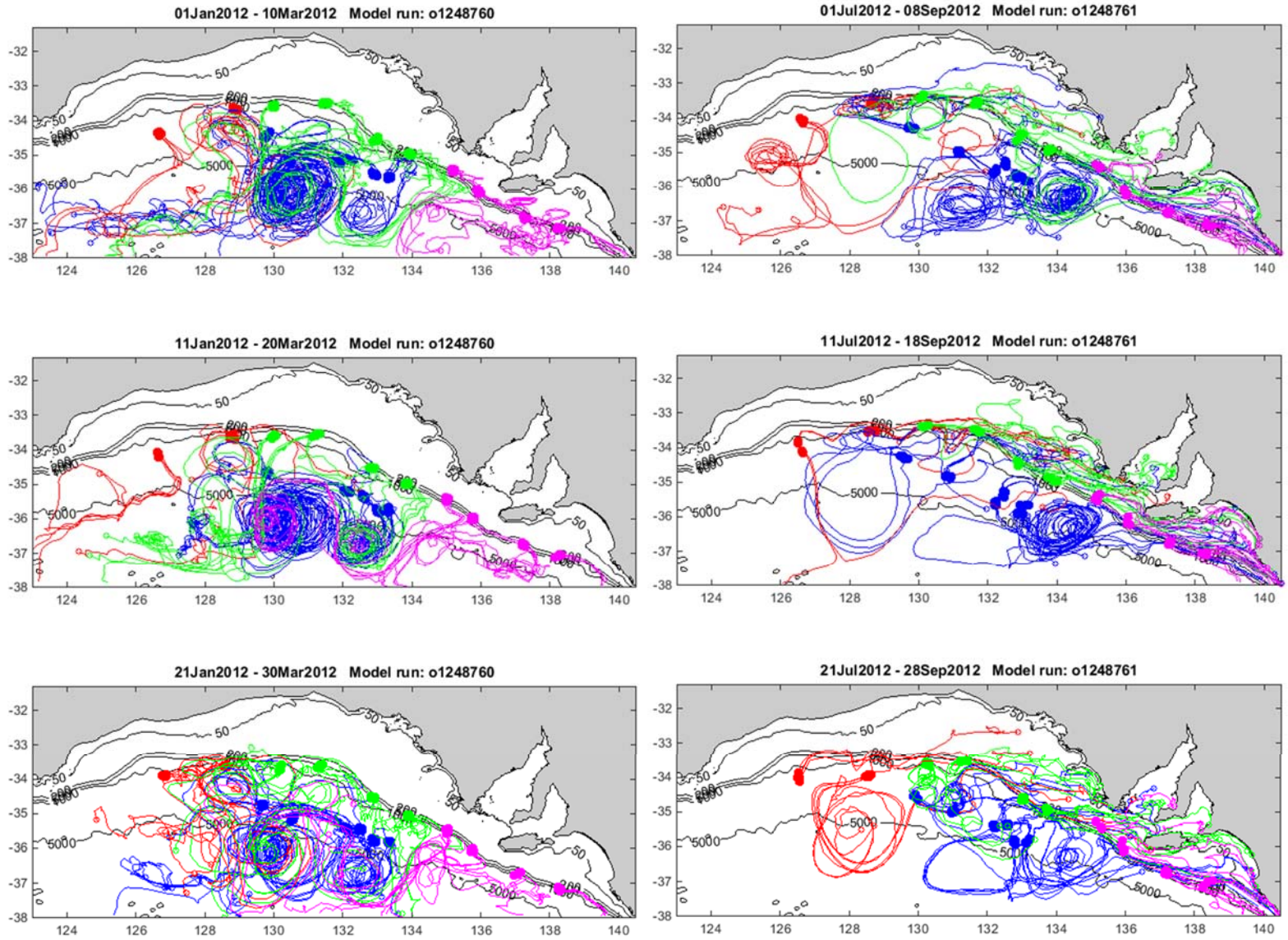

Figure 167: ROMs winter and summer offshore seeded particle trajectories using currents only for 2012.

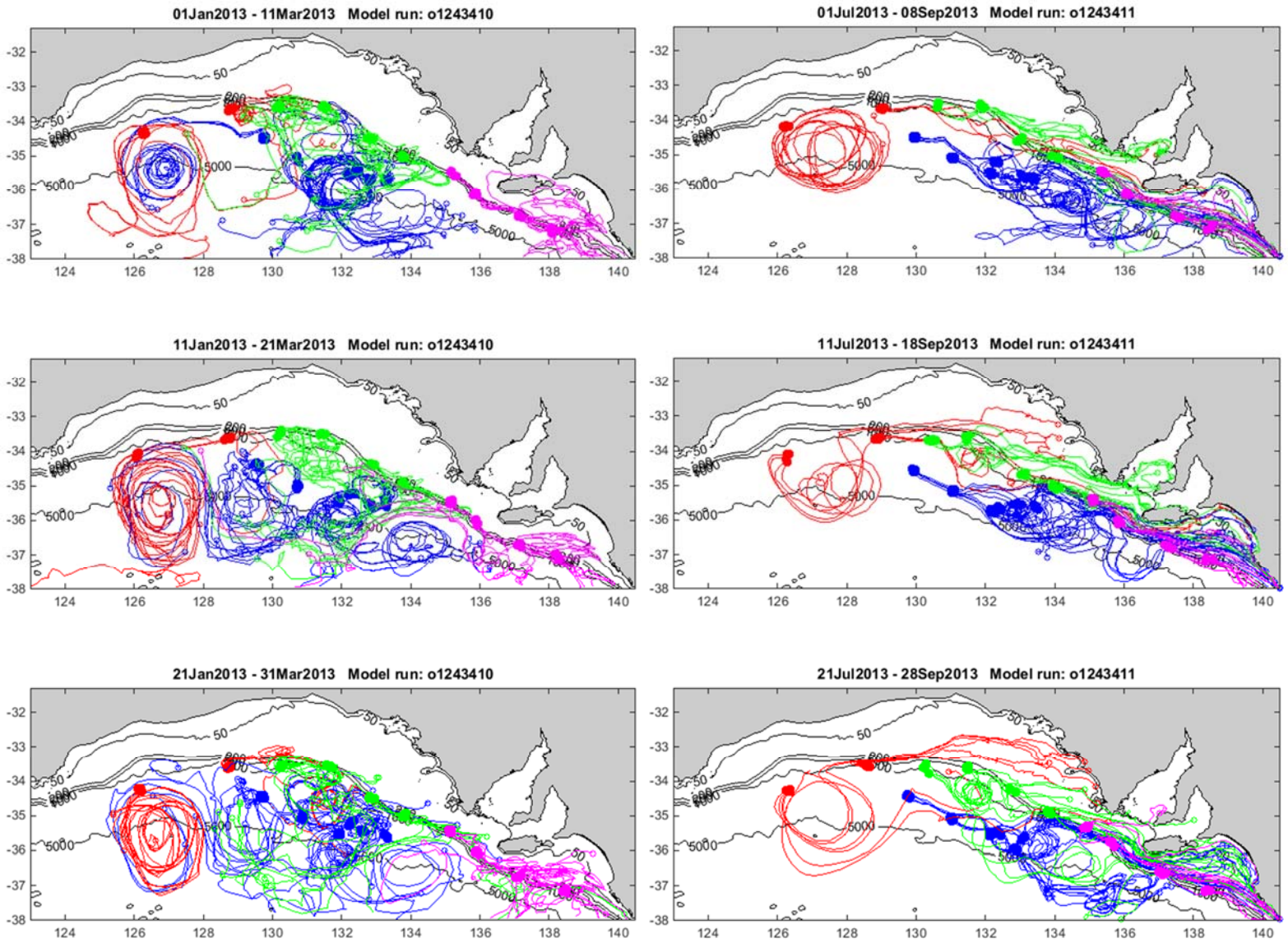

Figure 168: ROMs winter and summer offshore seeded particle trajectories using currents only for 2013.

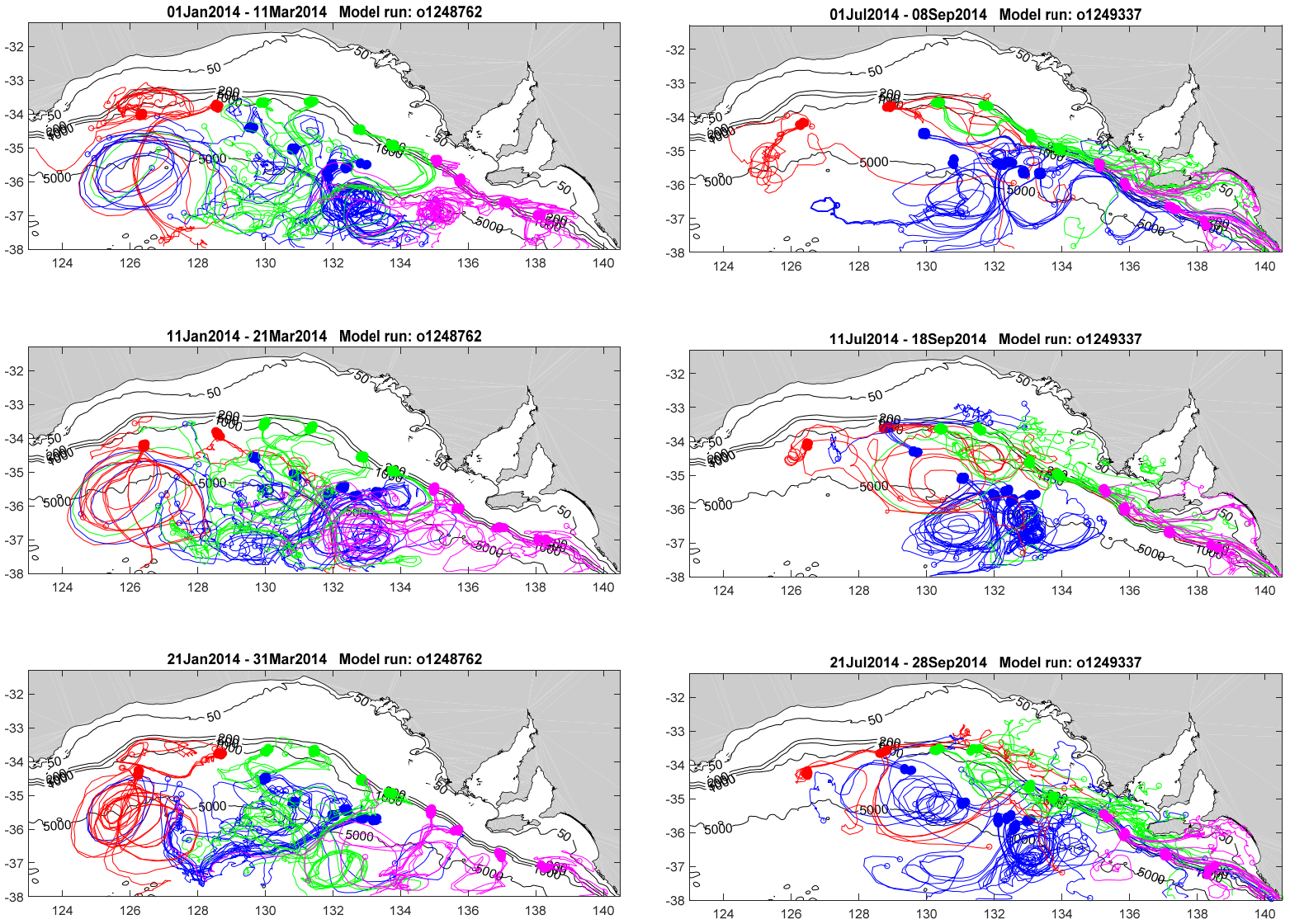

Figure 169: ROMs winter and summer offshore seeded particle trajectories using currents only for 2014.

Scenario 2 - Offshore seeded particle trajectories using currents and Stokes drift

The BRAN2015 modelling of offshore seeded particle trajectories over two-month and three-month periods between January 2011 and December 2016 once again showed significant differences between winter and summer trajectories across all of the years modelled. In addition, these modelling results also differ significantly from those derived from the ROMS model.

The BRAN2015 two-month and three-month model results for 2014 to 2016 are shown in Figure 170 to Figure 175, respectively. The modelling results for 2011 to 2013 are included in APPENDIX 8: BRAN MAPS FOR 2011, 2012 and 2013. As with the ROMS models winter processes (July, August and September) they display a number of general trends in the model iterations, which are summarized below:

a) Onshore surface Ekman transport;
b) Offshore shelf transport;
c) Shelf/slope exchange with the waters of Spencer Gulf;
d) General eastward flow including the Leeuwin Current (LC) (maximum over shelf break); and
e) Offshore eddies with diameters of 100-200 km.

Particle trajectories from the offshore seeding locations for 2014 (Figure 170 and Figure 173), 2015 (Figure 171 and Figure 174) and 2016 (Figure 172 and Figure 175) all show that the combined surface and Stokes drifts can lead to stranding of materials on the southern ends of the Eyre, Yorke and Fleurieu peninsulas, on Kangaroo Island, and along the Coorong and Limestone Coasts. The largest number of particle tracks appear to terminate along the Limestone Coast and to the east.

As the ROMS and BRAN2015 models are constructed differently their outputs would be expected to be slightly different if the same input parameters were used. However, with the additional parameters entered into these models, the model outputs would be expected to be quite different. The BRAN2015 and ROMS winter results are broadly consistent and can be directly compared using the 2014 data (Figure 169 and Figure 170). This comparison suggests that the Stokes drift is not a major component of the predominant processes in the GAB at this time (i.e. Leeuwin Current > Stokes drift component), and could further suggest that the two forces in the model are synergistic (i.e. they occur in the same orientation). This modelling outcome is consistent with observations of the Leeuwin Current movement and the winds associated with the storms that move from west to east across the GAB in the winter months.

As with the ROMS model, the BRAN2015 model show significant inter-annual variation. Some model iterations show particle stranding across much of the Eyre Peninsula, but not into the Head of the Bight, whilst other model iterations have little or no stranding along the Eyre Peninsula.

The autumn (April, May, June) BRAN2015 particle trajectories yield very similar results to those observed in the winter models. This is consistent with the strongest Leeuwin Current velocities occurring between autumn and winter.

To determine what the typical April–September trajectory patterns were across the years, a cumulative heat map that sums all particle trajectories across a 37 km grid for all modelled years was produced (see Figure 176). This figure confirms that the particle trajectories for this time of the year are consistent throughout the modelled period (2011-2016) and would lead to stranding of materials

at the southern ends of the Eyre, Yorke and Fleurieu peninsulas, on Kangaroo Island and along the Coorong and Limestone Coast, but not on beaches along the northern section of the Eyre Peninsula or the Head of the Bight.

The summer model iterations (January, February, March) show very different particle trajectories to those produced for the winter. The general trends based on the seeding locations in the model iterations are summarised below:

a) Onshore transport through Stokes drift as a result of strong to very strong onshore winds;
b) Shelf/slope blockage with the waters of Spencer Gulf;
c) Weak to absent Leeuwin Current;
d) Westward current in the Head of the Bight; and
e) Offshore eddies with diameters of 100-200km.

Particle trajectories from the offshore seeding locations for 2014 (Figure 170 and Figure 173), 2015 (Figure 171 and Figure 174) and 2016 (Figure 172 and Figure 175) show that the combined processes of surface currents and Stokes drift can lead to stranding across the whole study area including the Head of the Bight. In particular, they permit the stranding of materials along the whole of the Eyre Peninsula including in the vicinity of Dogfence Beach.

These BRAN2015 results differ very significantly from those produced using the ROMS model (see Figure 169 and Figure 170) and illustrates that Stokes drift is one of the predominant processes affecting the modelled particles during this period (i.e. Leeuwin Current < Stokes drift component). The Stokes drift during this time of the year is created by the forcing on the sea surface by strong winds that blow towards the north and northwest. These results are important as they provide a mechanism for the carriage of coastal bitumens from potential offshore seeding locations into the Head of the Bight, without which their transport to this area would be much more indirect. It is therefore considered that the BRAN2015 model which incorporates Stokes drift has a greater level of predictive power to determine possible stranding locations from offshore seeding origins.

As was the case for the winter models, there is significant inter-annual variation between summer models with some iterations showing predominant stranding along the West Australian coast and other years showing stranding more uniformly across the Head of the Bight.

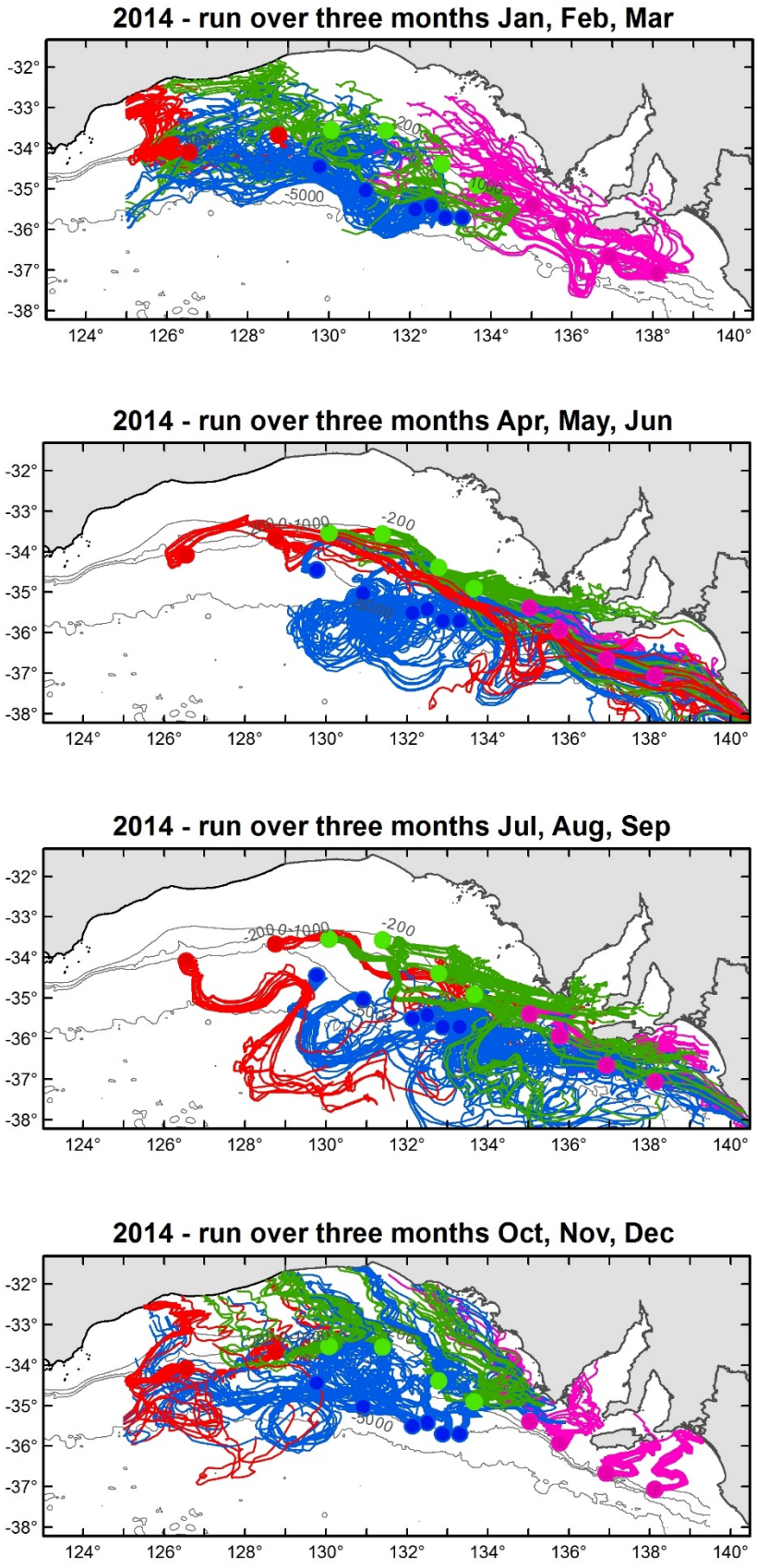

Figure 170: BRAN2015 three-monthly offshore seeded particle trajectories combining surface currents and Stokes drift for 2014.

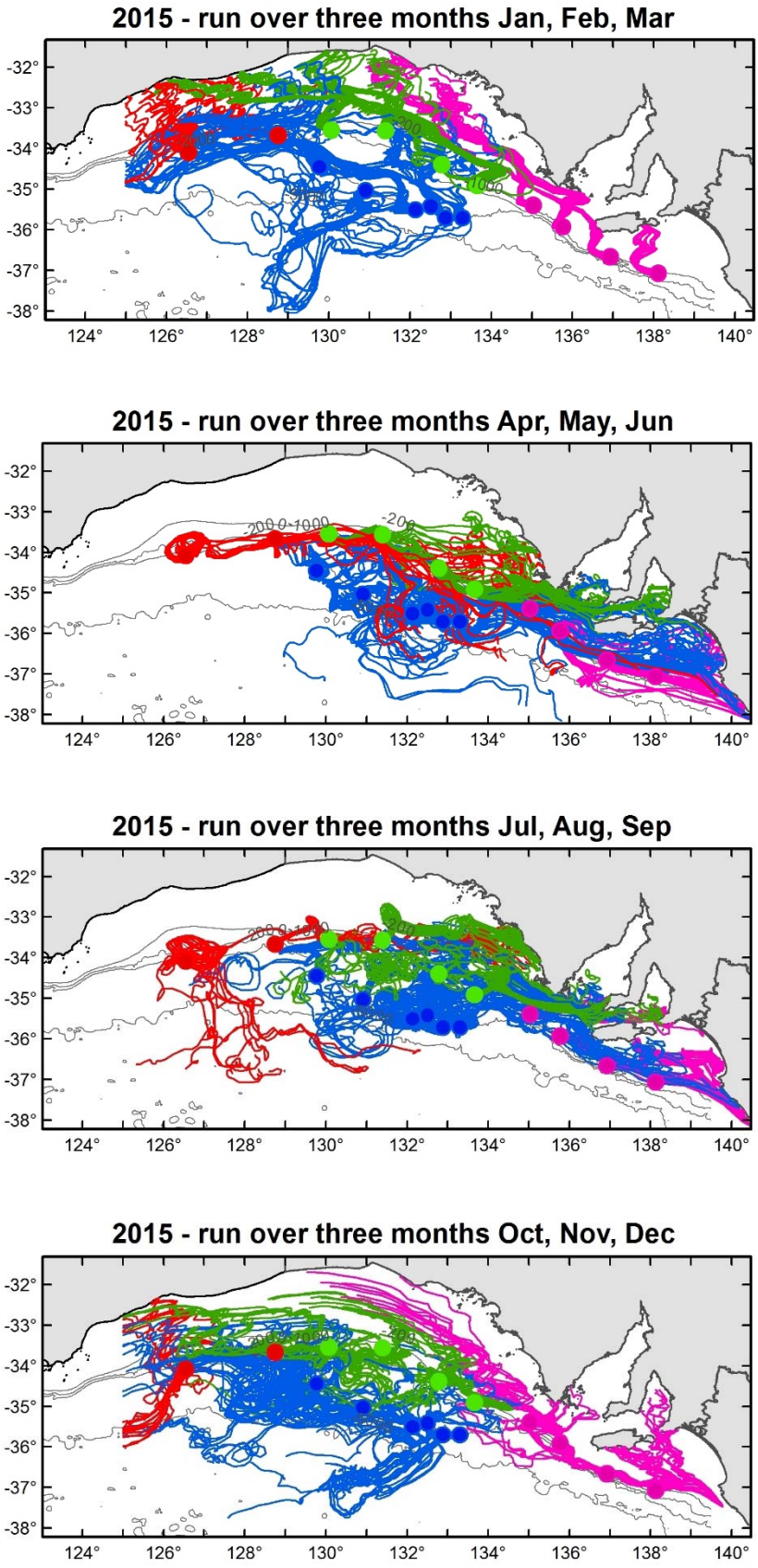

Figure 171: BRAN2015 three-monthly offshore seeded particle trajectories combining surface currents and Stokes drift for 2015.

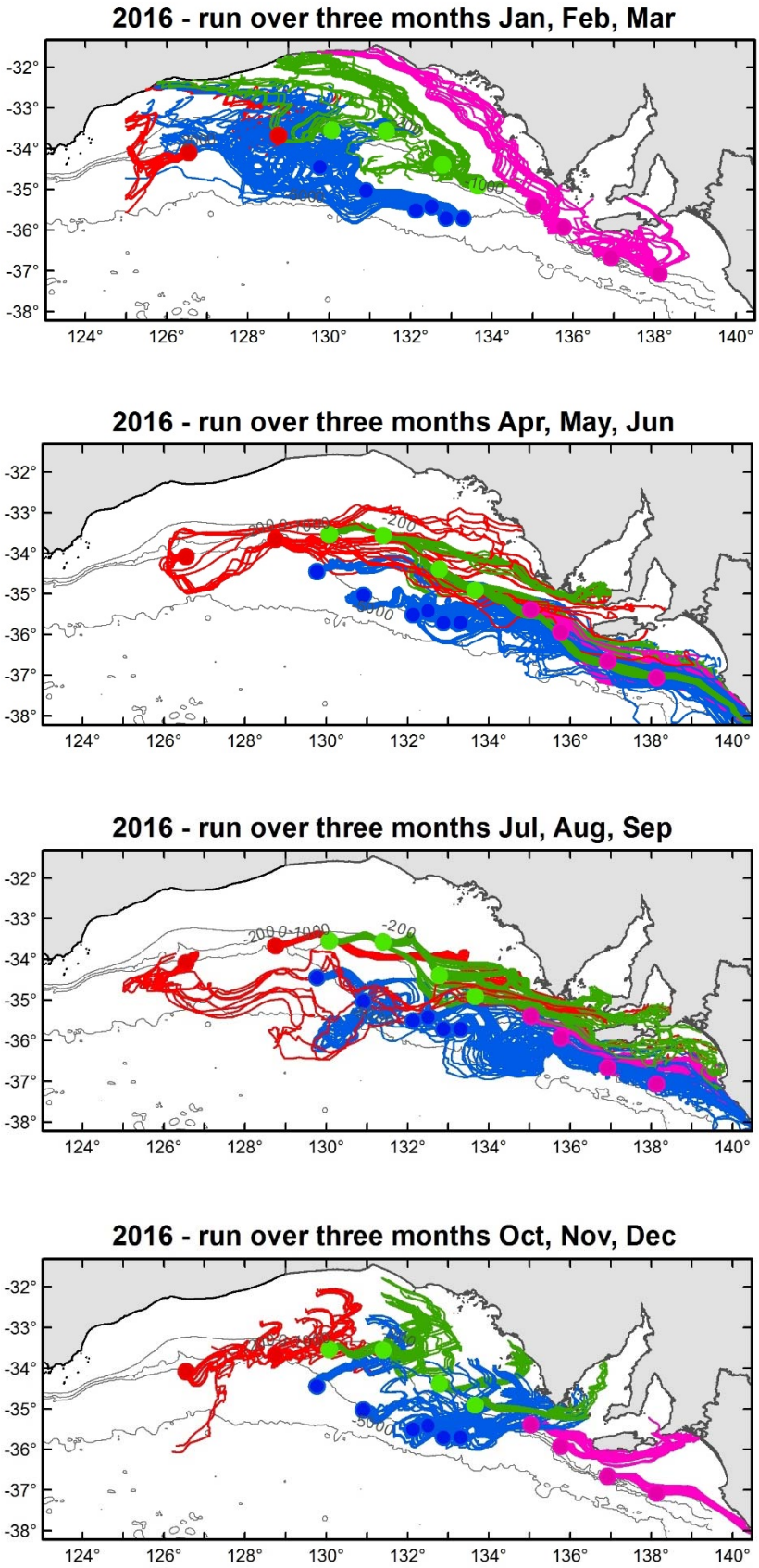

Figure 172: BRAN2015 three-monthly offshore seeded particle trajectories combining surface currents and Stokes drift for 2016.

The spring (October, November, December) particle trajectories yield results with some similarities to those observed during the summer models. However, the distribution of particle trajectories are more likely to encounter the beaches of the Eyre Peninsula (Figure 170-172). These trajectories are likely the result of the interplay between the waning Leeuwin Current during October and November and the strengthening onshore winds which drive Stokes drift. This can be observed in the two-month model results (Figure 173-175), wherein the September and October models show a predominantly winter trajectory pattern while the November and December models show a mainly summer trajectory pattern. Exceptions are the November and December 2016 model results, where north to north-easterly winds may not have been established, leading to a lack of particle movement when the Leeuwin Current intensity was low.

To illustrate the average October-March trajectory patterns across years, a cumulative heat map, that sums all particle trajectories across a 37-km grid for all modelled years is shown in Figure 177. This figure confirms that the particle trajectories during this period for 2011–2016 enter the central Bight and lead to a high frequency of trajectories encountering its western shorelines, Kangaroo Island, Fleurieu Peninsula and the Limestone Coast. There is also a moderate encounter rate with the shorelines of the Eyre Peninsula.

When particle seeding locations and their associated trajectories are considered for the forward track BRAN2015 models incorporating Stokes drift across the 2013–2016 annual cycles a number of patterns become apparent.

For particles seeded over the Eyre sub-basin and the most westerly extent of the Ceduna sub-basin (red points), the trajectories can lead to stranding locations from the mid-Eyre Peninsula through to through to the Limestone Coast during the winter conditions. However, the particles which are released during summer conditions are typically transported to the north and stranded on Western Australian beaches. Particles released from these locations only relatively infrequently enter the Head of the Bight and encounter the northern beaches of the Eyre Peninsula.

Particles released on the shelf break of the Ceduna sub-basin (green points) typically encounter the southern tip of the Eyre Peninsula through to the Limestone Coast during winter conditions, whilst during summer conditions these particles are more likely to travel to the west and encounter the cliff-lined coast of the western Bight. During spring these particle trajectories may encounter the whole of the Eyre Peninsula and the Head of the Bight, particularly those particles which are released along the eastern section of the Ceduna sub-basin shelf break.

Particles released from the deepwater continental slope of the Ceduna sub-basin (blue points) typically remain offshore throughout the duration of the model runs, entrained within offshore meso-scale eddies. Where encounters are made with shorelines, these are most frequently observed along the Limestone Coast during winter conditions or along the cliffs lining the western section of the Head of the Bight. During atypical conditions (e.g. October 2016) these particles can encounter shorelines along the Eyre Peninsula.

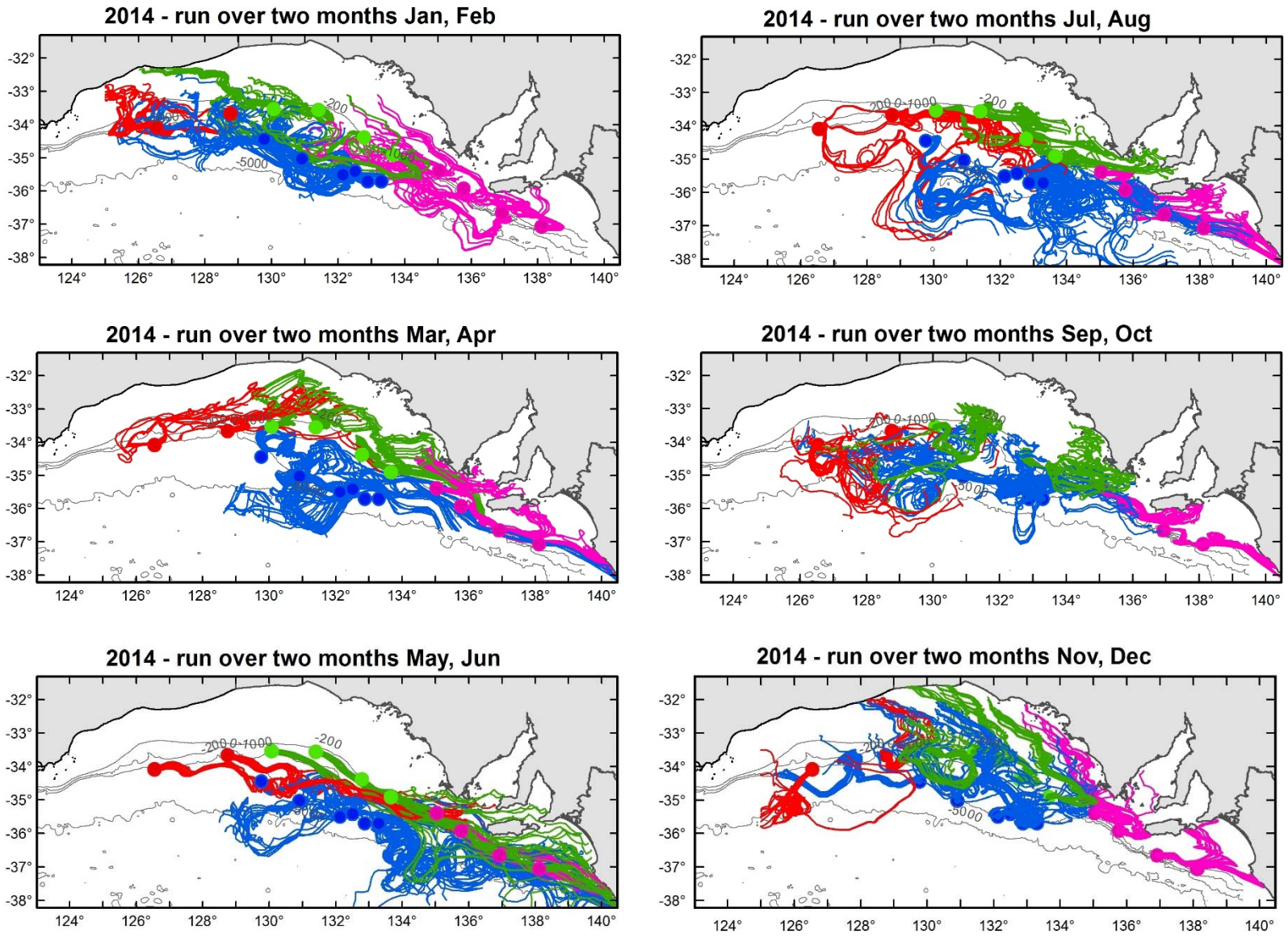

Figure 173: BRAN2015 two-monthly offshore seeded particle trajectories combining surface currents and Stokes drift for 2014.

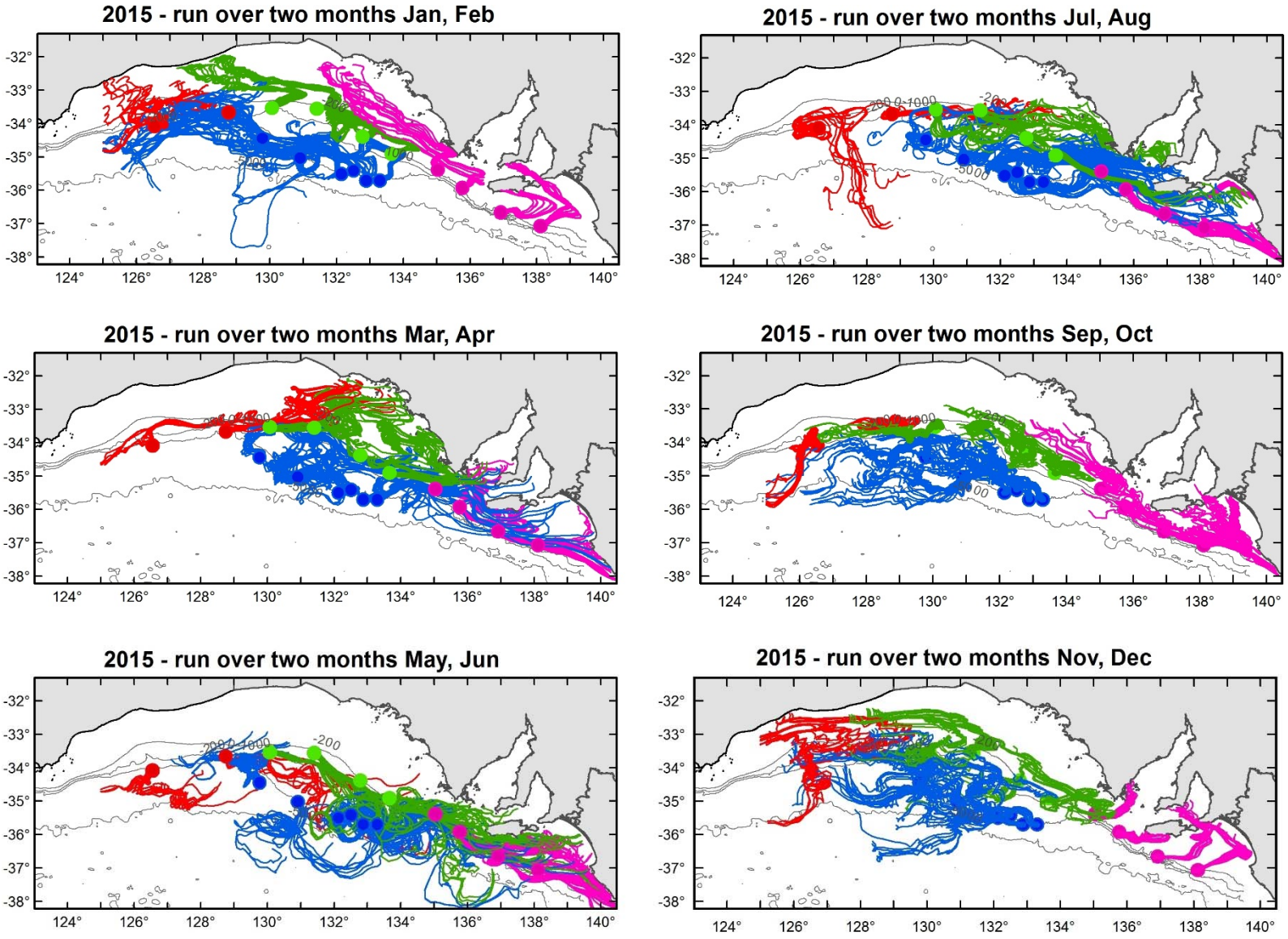

Figure 174: BRAN2015 two-monthly offshore seeded particle trajectories combining surface currents and Stokes drift for 2015.

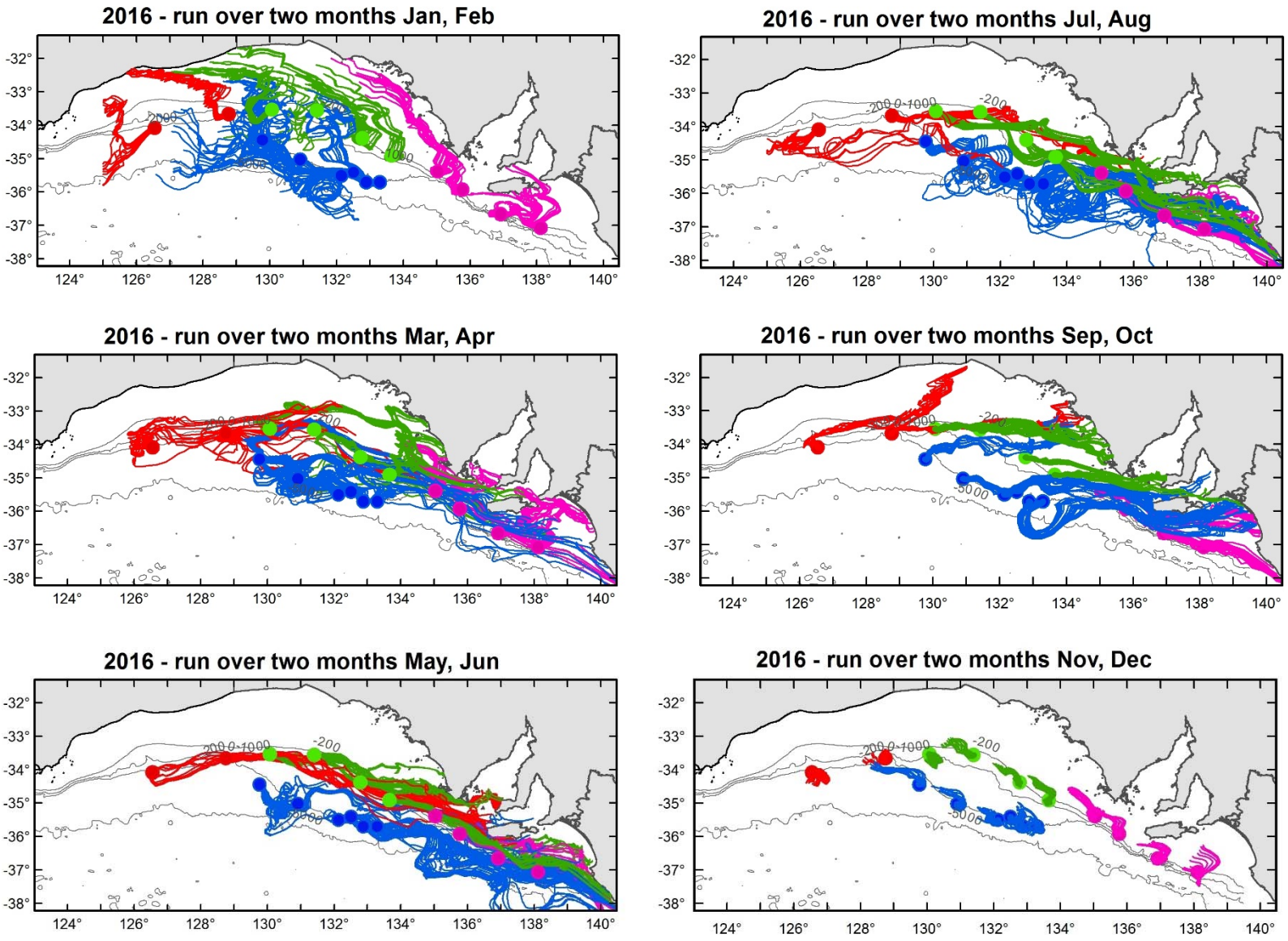

Figure 175: BRAN2015 two-monthly offshore seeded particle trajectories combining surface currents and Stokes drift for 2016.